The Canadian Mineralogist
Vol. 50, pp. 825-841 (2012)
DOI: 10.3749/canmin.50.4.825

ZONED REE-ENRICHED DRAVITE FROM A GRANITIC PEGMATITE IN FORSHAMMAR, BERGSLAGEN PROVINCE, SWEDEN: AN EMPA, XRD AND LA–ICP–MS STUDY

PETER BAČÍK§ AND PAVEL UHER

Comenius University in Bratislava, Faculty of Natural Sciences, Department of Mineralogy and Petrology, Mlynská dolina, SK–842 15 Bratislava, Slovak Republic

ANDREAS ERTL

Institut für Mineralogie und Kristallographie, Geozentrum, Universität Wien, Althanstraße 14, A–1090 Wien, Austria

ERIK JONSSON

Geological Survey of Sweden, Box 670, SE–751 28 Uppsala, Sweden, and Department of Earth Sciences, Uppsala University, SE–752 36 Uppsala, Sweden

PER NYSTEN

Geological Survey of Sweden, Box 670, SE–751 28 Uppsala, Sweden

VIKTOR KANICKÝ

Department of Chemistry, Faculty of Science, Masaryk University, Kotlářská 2, CZ–611 37 Brno, Czech Republic

TOMÁŠ VACULOVIČ

Central European Institute of Technology, Masaryk University, Kamenice 5, CZ–625 00 Brno, Czech Republic

ABSTRACT

Green to grayish green tourmaline crystals (up to 10 cm across), with distinct optical zoning, occurs with quartz, blocky albite and muscovite in the Forshammar granitic pegmatite, central Bergslagen province, Sweden. Tourmaline contains inclusions of zircon and xenotime-(Y), and it is cut by veinlets of muscovite and hydroxylbastnäsite-(Ce). Microanalytical and structural data (from the rim) indicate that the tourmaline can be classified as a dravite with moderate Al–Mg disorder at the *Y* and *Z* sites. Tourmaline displays chemical zoning that reflects the distribution of Fe, Mg, Al, Ca and Na. The Mg/(Mg+Fe) value is high; it decreases from core (~0.85) to intermediate zone (0.76–0.79), but increases in the rim and vein dravite (0.93). The core has the highest proportion of *X*-site vacancy and Al content, whereas the intermediate zone is the most enriched in Fe and Na. The rim is slightly depleted in Al and has the highest Na compared to inner zones. Tourmaline veins crosscut the pre-existing tourmaline and are relatively more enriched in Na and Ca. The main compositional variations are driven by $Al^{X}\square Mg_{-1}Na_{-1}$ and $AlOMg_{-1}(OH)_{-1}$ substitutions. The Forshammar dravite shows the highest known concentrations of REE from pegmatite tourmaline, ≤1200 ppm REE, ≤210 ppm La, ≤670 ppm Ce; the chondrite-normalized patterns reveal high La_N/Yb_N (32 to 464) values and strongly negative Eu anomalies (Eu/Eu* = 0.005 to 0.05). The contents of Ti, Mn, Y and REE generally increase at the boundary of the intermediate zone and rim, whereas the contents of Zn, Ga and Sn decrease from the core to the rim. The core is likely a product of an early magmatic process during the late Svecofennian pegmatite formation (~1.8 Ga) as suggested by oscillatory zoning of trace elements. The intermediate zone, rim and tourmaline veins originated during the late magmatic to hydrothermal stage. Hydroxylbastnäsite-(Ce) and muscovite are apparently the final products of the hydrothermal process.

Keywords: tourmaline, dravite, muscovite, zircon, xenotime-(Y), hydroxylbastnäsite-(Ce), REE, EMPA, XRD, LA–ICP–MS, granitic pegmatite, Forshammar, Bergslagen, Sweden.

§ *E-mail address*: bacikp@fns.uniba.sk

Introduction

Dravite, a magnesium-dominant alkali tourmaline, is a relatively widespread mineral, mainly in metamorphic and metasedimentary rocks, especially in metapelites to metapsammites, amphibole gneisses, marbles, dolomites, and skarns. In contrast, dravite is not typical of common granitic pegmatite environments, where schorl-to-foitite and elbaite members of the tourmaline supergroup are the most widespread (*e.g.,* London 2008). Magnesium-rich members of the schorl–dravite solid-solution series occur only in very primitive barren granitic pegmatites or in relatively unusual Mg-rich environments, such as desilicated pegmatites emplaced in (ultra)basic rocks (*e.g.,* Bernard & Hyršl 2006) or NYF pegmatites derived from Mg-rich parental plutonic rocks, *e.g.,* melasyenites to melagranites of the Třebíč Pluton, Czech Republic (Novák *et al.* 2011).

In this contribution, we document an occurrence of distinctly Mg-rich dravite with unusually high REE contents and associated minerals from a granitic pegmatite at Forshammar, Bergslagen ore province, central Sweden. We carried out a detailed X-ray powder and single-crystal study with a crystal-structure refinement, supplemented by EMPA (electron microprobe) and LA–ICP–MS (laser ablation – inductively coupled plasma – mass spectrometry) spot analyses to establish the internal evolution of the tourmaline from the magmatic to subsolidus stage.

Geological Setting and Occurrence

The Forshammar area is situated in the western central part of the Paleoproterozoic, *ca.* 2.0–1.8 Ga Bergslagen ore province (Fig. 1). The main metasupracrustal sequence in Bergslagen consists of Svecofennian volcano-sedimentary units dominated by rhyolitic-to-rhyodacitic, alkali-enriched metavolcanic rocks, clastic metasediments, calcite-rich to dolomite-rich marbles, and minor metabasic dykes and flows. The felsic metavolcanic rock units formed primarily in a volcanic arc environment at *ca.* 1.90–1.87 Ga (*cf.* Lundström *et al.* 1998, and references therein), and the sequence was subjected to intense folding, faulting and regional metamorphism during the Svecokarelian orogeny, as well as to the intrusion of large volumes of mostly granitic magma during several successive stages. The resulting rocks have been historically divided into an older and a younger series; characteristically, the younger series is dominated by mostly undeformed granites of overall S-type affinity, as exemplified by the *ca.* 1.8 Ga Stockholm granite (Ivarsson & Johansson 1995, and references therein). The vast majority of rare-element-type granitic pegmatites in central Sweden formed during *ca.* 1.82–1.79 Ga (*cf.* Romer & Smeds 1997), thus overlapping in time with these granites.

Overall, the region around Forshammar hosts abundant pegmatitic to granitic bodies, occurring on several scales, from thin dykes to large pods. They are considered to belong to the *ca.* 1.8 Ga generation of granites, and are mostly mineralogically simple and unzoned, and dominated by coarse-grained quartz–feldspar rocks with smaller amounts of micas and locally also magnetite (Sundius 1952, Ambros 1983). At some localities, they form distinct pegmatitic units, with a coarse to very coarse grain-size, typically with very coarse radial aggregates of muscovite, and irregularly distributed small (decimeter- to meter-sized) pods of quartz. A relatively coarse-grained graphic intergrowth between quartz and perthitic microcline is generally dominant. Several of these larger pegmatite bodies have been mined, primarily for feldspar, such as in the Klinttjärnbo and Limbergsbo quarries (K and L, respectively, in Fig. 1), in the Forshammar area. The Limbergsbo quarry is still in operation.

The granitic pegmatites of the area are, to a large extent, hosted by felsic metavolcanic units, in contrast to a majority of pegmatite fields in central Sweden. Furthermore, pegmatites are characteristically Al-rich, shown by the fairly widespread occurrence of andalusite (Flink 1917, Lundegårdh 1971), and the sporadic appearance of chrysoberyl. Mineralogically unspecified tourmaline-supergroup minerals have been observed in the Forshammar pegmatites, as previously noted by Brotzen (1959) and Lundegårdh (1971). The latter author specifically noted the occurrence of "light gray tourmalines" from the Forshammar quarries. Yet, on the basis of observations during a succession of visits to the area, tourmaline must be considered a rare constituent of these pegmatites. Variably altered andalusite, sparse molybdenite and occasional small amounts of an unspecified, black allanite-like mineral have also been noted (*cf.* Lundegårdh 1971).

We sampled a tourmaline-bearing pegmatite body (GPS geographic coordinates: 59°46'6"N, 15°30'56"E) situated about 1 km northeast of the Klinttjärnbo quarry in the Forshammar area, exposed in relatively recent times through road construction work. In the remaining exposed portion of the pegmatite, a half-meter-size local quartz core occurs within a muscovite-bearing, coarse-grained graphic intergrowth of K-feldspar and quartz. The euhedral prismatic tourmaline crystals occur at the boundary or immediately inside the quartz at the core margin, in some cases projecting some 10 centimeters into the quartz core. A large part of this particular small core is asymmetrically filled by a single, euhedral and megacrystic internally graphic K-feldspar crystal.

Analytical Methods

Electron-microprobe analysis (EMPA)

The composition of tourmaline and associated minerals was established with a CAMECA SX100 electron microprobe in wavelength-dispersion mode at the State Geological Institute of Dionýz Štúr, Bratislava,

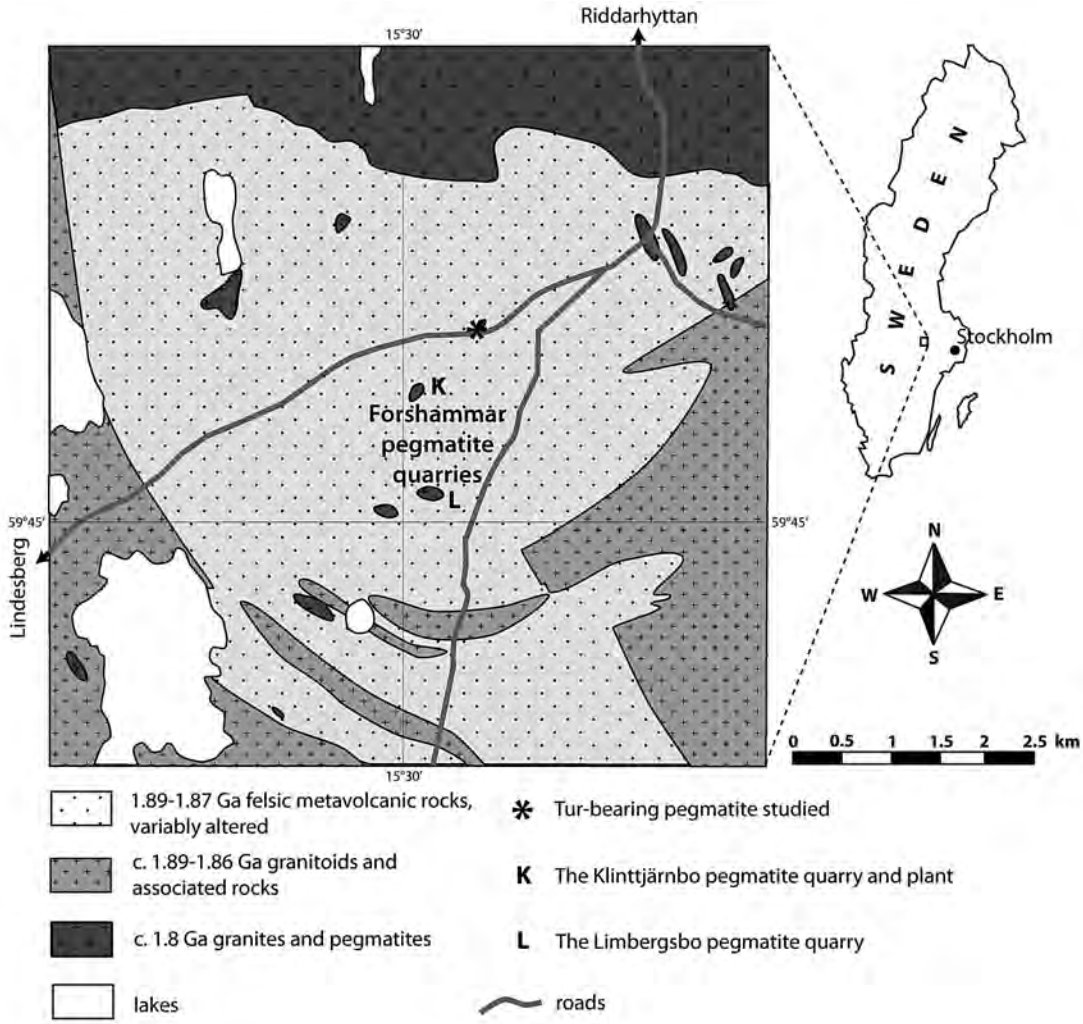

FIG. 1. Simplified geological map of the bedrock in the Forshammar area. The map is based on data from the Geological Survey of Sweden, including the findings of Ambros (1983).

under the following conditions: accelerating voltage 15 keV, beam current 20 nA, and beam diameter 3 to 5 μm. The tourmaline samples were analyzed with the following standards: wollastonite (Si$K\alpha$, Ca$K\alpha$), TiO_2 (Ti$K\alpha$), Al_2O_3 (Al$K\alpha$), pure Cr (Cr$K\alpha$), pure V (V$K\alpha$), fayalite (Fe$K\alpha$), rhodonite (Mn$K\alpha$), forsterite (Mg$K\alpha$), willemite (Zn$K\alpha$), pure Ni (Ni$K\alpha$), albite (Na$K\alpha$), orthoclase (K$K\alpha$), BaF_2 (F$K\alpha$) and NaCl (Cl$K\alpha$). The lower limits of detection of the measured elements vary between 0.01 and 0.05 wt.%; Zn, Ni and Cl were invariably found to be below their detection limits. The analytical data were normalized according to the PAP procedure. The calculation procedure of tourmaline formula is presented in Table 1. Analytical details on the electron-microprobe measurements of zircon, xenotime-(Y) and hydroxylbastnäsite-(Ce) are given in Pršek *et al.* (2010).

Powder X-ray diffraction

Powder X-ray-diffraction analyses were made on a BRUKER D8 Advance diffractometer (Laboratory of X-ray diffraction SOLIPHA, Comenius University in Bratislava, Faculty of Natural Sciences) under following conditions: Bragg–Brentano geometry (θ–2θ), Cu anticathode ($\lambda\alpha_1$ = 1.54060 Å), accelerating voltage 40 kV, beam current 40 mA. We used Ni $K\beta$ filters to strip the $K\beta$ radiation on the primary and diffracted beam,

and data were obtained with the BRUKER LynxEye detector. The step size was 0.01° 2θ, the step time was 5 s per step, and the range of measurement was 4 – 65° 2θ. The measured data were evaluated with the DIFFRAC^{plus} EVA software package (Bruker 2010a). Analyzed scans were fitted and lattice parameters were refined with the DIFFRAC^{plus} TOPAS software using a pseudo-Voight function (Bruker 2010b).

Crystal-structure refinement

A fragment of the rim (sample TSW an3) of a tourmaline crystal (originally ~5 cm in length) from Forshammar was examined on a Kappa APEX II CCD single-crystal X-ray diffractometer from Bruker AXS equipped with a monocapillary optics collimator, graphite-monochromatized Mo$K\alpha$ radiation (Universität Wien). Data were collected at room temperature with six-fold redundancy (up to 80° 2θ), integrated and corrected for Lorentz and polarization factors; an absorption correction was applied by evaluation of multiple scans. The structure was refined with SHELXL–97 (Sheldrick 1997) using scattering factors for neutral atoms and a tourmaline starting model from Ertl *et al.* (2010b). The refinement converged at $R1(F)$ value of 1.5%. Table 2 provides crystal data and details of the structure refinement. The H atom bonded to the O3 atom was located from a difference-Fourier map and subsequently refined. Refinement was performed with anisotropic thermal parameters for all non-hydrogen atoms. Site occupancies were refined according to well-known characteristics of the tourmaline structure (Na was refined at the *X* site, and Mg and Fe were refined at the *Y* site; for further details see Table 3). In Table 3, we list the atomic parameters, and in Table 4 we present selected interatomic distances. A table of structure factors and a cif file are available from the Depository of Unpublished Data on the Mineralogical Association of Canada website [document Dravite CM50_825].

TABLE 1. REPRESENTATIVE COMPOSITIONS OF DRAVITE FROM FORSHAMMAR, BERGSLAGEN PROVINCE, SWEDEN

	TSW an13 core	TSW an44 core	TSW an10 int. z.	TSW an14 int. z.	TSW an3 rim	TSW an5 rim	TSW an47 vein	TSW an50 vein
SiO_2	37.90	38.27	37.32	37.76	37.97	38.14	38.47	38.24
TiO_2	0.08	0.09	0.16	0.14	0.18	0.14	0.01	0.01
B_2O_3*	11.03	11.05	10.92	10.99	11.01	11.04	11.05	11.02
Al_2O_3	36.11	35.92	35.24	35.34	34.78	34.91	33.67	33.47
FeO	2.62	2.48	3.58	3.38	1.23	1.22	1.37	1.31
MnO	0.05	b.d.l.	0.06	0.07	0.05	b.d.l.	b.d.l.	b.d.l.
MgO	7.80	7.76	7.67	7.63	9.24	9.31	10.23	10.37
CaO	0.03	0.02	0.08	0.04	0.30	0.27	0.51	0.69
Na_2O	1.81	1.91	2.23	2.35	2.32	2.26	2.32	2.35
K_2O	0.04	0.03	0.03	0.04	0.05	0.04	b.d.l.	b.d.l.
H_2O*	3.42	3.31	3.32	3.26	3.25	3.29	3.33	3.28
F	b.d.l.	b.d.l.	0.13	0.07	0.08	0.08	0.23	0.27
Total	100.89	100.90	100.79	101.12	100.49	100.72	101.23	101.07
Si *apfu*	5.974	6.020	5.939	5.974	5.995	6.004	6.053	6.033
Al	0.026	0.000	0.061	0.026	0.005	0.000	0.000	0.000
Σ*T*	6.000	6.020	6.000	6.000	6.000	6.004	6.053	6.033
B	3.000	3.000	3.000	3.000	3.000	3.000	3.000	3.000
Ti	0.009	0.011	0.019	0.017	0.022	0.017	0.001	0.001
Al	6.682	6.658	6.548	6.564	6.467	6.476	6.244	6.224
Fe	0.345	0.327	0.477	0.447	0.163	0.160	0.181	0.173
Mn	0.006	-	0.008	0.009	0.006	0.002	-	-
Mg	1.833	1.820	1.820	1.798	2.174	2.185	2.400	2.439
Σ*Y*+*Z*	8.875	8.815	8.871	8.835	8.832	8.841	8.826	8.837
Ca	0.005	0.004	0.013	0.006	0.050	0.046	0.086	0.116
Na	0.554	0.582	0.687	0.722	0.711	0.689	0.706	0.718
K	0.007	0.006	0.006	0.007	0.010	0.007	0.005	0.004
$^{X}\square$	0.434	0.408	0.294	0.265	0.228	0.258	0.203	0.161
Σ*X*	0.566	0.592	0.706	0.735	0.772	0.742	0.797	0.839
F	-	-	0.067	0.036	0.038	0.041	0.114	0.134
OH	3.597	3.474	3.527	3.439	3.420	3.451	3.495	3.455
O	0.403	0.526	0.406	0.523	0.542	0.507	0.390	0.411
Σ*V*+*W*	4.000	4.000	4.000	4.000	4.000	4.000	4.000	4.000
ΣCat.	18.444	18.433	18.583	18.577	18.608	18.588	18.679	18.714
ΣAl	6.708	6.658	6.609	6.590	6.473	6.476	6.244	6.224

The analytical data, acquired with an electron microprobe, is first reported in wt.%, and then converted to atoms per formula unit on the basis of 15 cations per formula unit. A component is not considered significant unless its value exceeds the uncertainty (b.d.l.: below detection limit). * B_2O_3 was calculated assuming 3.00 *apfu*; ** OH and $^{V+W}$O were calculated from the charge-balanced formula, H_2O was calculated for OH + O = 4 *apfu*. Notation: int. z.: intermediate zone.

Laser-ablation ICP–MS spot analysis (LA–ICP–MS)

Instrumentation for LA–ICP–MS analysis consists of a laser-ablation system UP 213 (New Wave, USA) and an Agilent 7500 CE ICP–MS spectrometer (Agilent, Japan). A commercial Q-switched Nd–YAG laser-ablation device works at the fifth harmonic frequency, which corresponds to a wavelength of 213 nm. The ablation device is equipped with programmable XYZ-stage to move the sample along a programmed trajectory during ablation. Visual inspection of the target and photographic documentation are accomplished by

TABLE 2. CRYSTALLOGRAPHICAL DATA AND REFINEMENT DETAILS FOR TOURMALINE FROM FORSHAMMAR

Sample	TSW an3 (rim)
a, *c* (Å)	15.921(1), 7.175(1)
V (Å^3)	1575.1(4)
Crystal dimensions (mm)	0.15 × 0.20 × 0.20
Collection mode, $2\theta_{max}$ (°)	full sphere, 80.24
h, *k*, *l* ranges	–28 → 25, –28 → 28, –13 → 12
Total reflections measured	23334
Unique reflections	2370 (R_{int} 2.14%)
$R_1(F)$, $wR_2(F^2)$	1.51%, 3.79%
Flack *x* parameter	0.060(44)
"Observed> reflections [$F_o > 4\sigma_{(Fo)}$]	2323
Extinction coefficient	0.00371(15)
Number of refined parameters	95
GooF	0.916
$\Delta\sigma_{min}$, $\Delta\sigma_{max}$ (e/Å^3)	–0.27, 0.36

TABLE 3. COORDINATES AND DISPLACEMENT PARAMETERS OF ATOMS IN TOURMALINE FROM FORSHAMMAR

Site	*x*	*y*	*z*	U_{11}	U_{22}	U_{33}	U_{23}	U_{13}	U_{12}	U_{eq}	Occupancy
X	0	0	0.2307	0.0191	0.0191	0.0197	0	0	0.0096	0.0193	$Na_{0.86(1)}$
			0.0002	0.0004	0.0004	0.0006			0.0002	0.0003	
Y	0.12439	½*x*	0.63110	0.00682	0.00470	0.01074	-0.00172	-0.00344	0.00341	0.0072	$Mg_{0.923(1)}Fe_{0.076}$
	0.00003		0.00005	0.00015	0.00011	0.00016	0.00005	0.00010	0.00007	0.0001	
Z	0.29771	0.26139	0.61062	0.00682	0.00470	0.01074	-0.00172	-0.00344	0.00341	0.00540	$Al_{1.00}$
	0.00002	0.00002	0.00003	0.00015	0.00011	0.00016	0.00005	0.00010	0.00007	0.00004	
B	0.10976	2*x*	0.4540	0.00528	0.00555	0.00533	0.00038	-0.00007	0.00267	0.0060	$B_{1.00}$
	0.00003		0.0002	0.00008	0.00008	0.00007	0.00006	0.00006	0.00007	0.0001	
T	0.19176	0.18981	-0.00040	0.00462	0.00423	0.00521	-0.00060	-0.00044	0.00220	0.00469	$Si_{1.00}$
	0.00001	0.00001	0.00003	0.00007	0.00007	0.00007	0.00006	0.00006	0.00005	0.00003	
H3	0.259	½*x*	0.402	0.0052	0.0057	0.0071	0.0007	0.00034	0.00286	0.034	$H_{1.00}$
	0.002		0.004	0.0003	0.0004	0.0004	0.0003	0.00014	0.00018	0.007	
O1	0	0	0.7716	0.0131	0.0131	0.0071	0	0	0.00655	0.0111	$O_{1.00}$
			0.0002	0.0003	0.0003	0.0005			0.00017	0.0002	
O2	0.06098	2*x*	0.4863	0.0126	0.0050	0.0127	0.0002	0.00010	0.00252	0.0110	$O_{1.00}$
	0.00003		0.0001	0.0003	0.0003	0.0003	0.0002	0.00011	0.00013	0.0001	
O3	0.26378	½*x*	0.5095	0.0246	0.0120	0.0057	0.00008	0.0002	0.0123	0.0127	$O_{1.00}$
	0.00008		0.0001	0.0004	0.0002	0.0003	0.00014	0.0003	0.0002	0.0001	
O4	0.09353	2*x*	0.0705	0.00715	0.0145	0.0097	-0.0015	-0.00075	0.00727	0.0096	$O_{1.00}$
	0.00003		0.0001	0.00019	0.0003	0.0003	0.0003	0.00013	0.00017	0.0001	
O5	0.18512	½*x*	0.0924	0.0150	0.00726	0.0093	0.00088	0.0018	0.00750	0.0097	$O_{1.00}$
	0.00007		0.0001	0.0003	0.00019	0.0003	0.00012	0.0002	0.00017	0.0001	
O6	0.19549	0.18515	0.77620	0.0093	0.0098	0.00527	-0.00128	-0.00083	0.00521	0.00792	$O_{1.00}$
	0.00004	0.00004	0.00007	0.0002	0.0002	0.00018	0.00015	0.00015	0.00017	0.00008	
O7	0.28536	0.28518	0.07831	0.00649	0.00625	0.00760	-0.00101	-0.00103	0.00121	0.00766	$O_{1.00}$
	0.00004	0.00004	0.00007	0.00019	0.00018	0.00019	0.00015	0.00015	0.00015	0.00008	
O8	0.20954	0.27033	0.43993	0.00467	0.0090	0.0118	0.00257	0.00093	0.00336	0.00851	$O_{1.00}$
	0.00004	0.00004	0.00008	0.00018	0.0002	0.0002	0.00016	0.00016	0.00016	0.00008	

Note: For the definition of U_{eq}, see Fischer & Tillmanns (1988).

TABLE 4. SELECTED INTERATOMIC DISTANCES IN TOURMALINE FROM FORSHAMMAR

X-	O2	×3	2.488(1)	*Y*-	O1		1.9894(8)
	O5	×3	2.739(1)		O2	×2	1.9911(6)
	O4	×3	2.824(1)		O6	×2	1.9953(6)
Mean			2.684(1)		O3		2.1108(11)
				Mean			2.0122(7)
T-	O7		1.6070(5)				
	O6		1.6071(6)	*Z*-	O6		1.8863(6)
	O4		1.6242(3)		O7		1.8984(6)
	O5		1.6394(4)		O8		1.8922(6)
Mean			1.6194(5)		O8'		1.9210(6)
					O7'		1.9532(6)
B-	O2		1.365(1)		O3		1.9889(5)
	O8	×2	1.3794(8)	Mean			1.9233(6)
Mean			1.375(1)				

The standard deviation is given in brackets. Distances are quoted in Å.

means of a built-in microscope–CCD camera system. The ablation cell was flushed with helium (carrier gas) that transported the laser-induced aerosol to the inductively coupled plasma. A sample gas flow of argon was admixed to the helium carrier gas flow behind the laser-ablation cell. Optimization of the LA–ICP–MS conditions (gas flow rates, sampling depth, voltages of electrostatic lenses of the mass spectrometer) was performed with the glass reference material NIST SRM 612 in order to obtain the maximum signal-to-noise ratio and minimum oxide formation (ThO^+/Th^+ counts ratio 0.2%, U^+/Th^+ counts ratio 1.1%). The hole-drilling mode (fixed position of the sample during laser ablation) was used for a duration of 40 seconds for each spot. Laser ablation was performed with a laser-spot diameter of 65 μm (samples TSW), laser fluence 13 J cm^{-2} and repetition rate 10 Hz. All element contents were normalized using Si as an internal standard. Its concentration was obtained by means of EMPA measurements.

RESULTS

Chemical composition, structure and zoning of tourmaline

Tourmaline from the pegmatite studied at Forshammar occurs as distinctly optically zoned crystals up to 10 cm in length and 2 cm in width, scattered in white quartz and white blocky albite. Tourmaline

crystals consist macroscopically of a green core and grayish green rim. Moreover, there is a darker green zone in between the core and rim observable in the thin section. Optical zoning is related to chemical zoning, as observed in back-scattered (BSE) images (Fig. 2a). Tourmaline crystals are cut by veins of younger tourmaline and even later veins of muscovite and hydroxylbastnäsite-(Ce) (Figs. 2b, c).

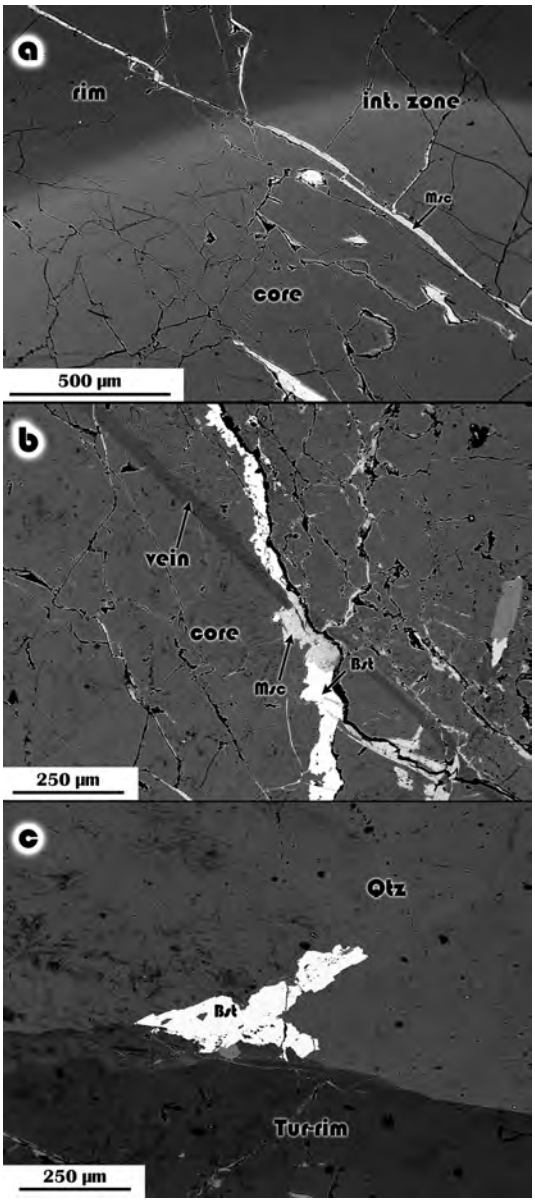

FIG. 2. BSE photomicrographs of dravite and associated minerals from the Forshammar pegmatite. (a) The contacts of the tourmaline core, intermediate zone and rim, cut by veins of muscovite (Ms). (b) Core of tourmaline cut by younger tourmaline vein and even later vein with muscovite and hydroxylbastnäsite-(Ce) (Bst). (c) Aggregate of hydroxylastnäsite-(Ce) in quartz (Qtz) growing on the rim of tourmaline (Tur-rim).

Microchemical data demonstrate that tourmaline from the Forshammar pegmatite belongs to the alkali subgroup (Fig. 3) and has a dravite composition, poor in Fe (Figs. 4b, d); the Mg/(Mg+Fe) value decreases from core (~0.85) to an intermediate zone (0.76–0.79), but increases in rim and vein dravite (0.93) (Table 1). In dravite from the Forshammar pegmatite, chemical zoning is the best displayed in the distribution of Fe, Mg, Al, Ca and Na, as well as in REE and other trace elements (see below). The core has the highest proportion of *X*-site vacancy (0.34–0.43) and the highest content of Al (6.62–6.71 *apfu*), whereas the intermediate zone is the most enriched in Fe (0.44–0.54 *apfu*) and Na (0.69–0.75 *apfu*), although the Mg content is similar in both zones (1.74–1.89 *apfu*) (Table 1). The rim is slightly depleted in Al (6.46–6.47 *apfu*), and it has the lowest content of Fe (0.16–0.18 *apfu*) and highest content of Mg (2.12–2.18 *apfu*) and Na (0.74–0.77 *apfu*) compared to the inner zones (Table 1). The latest thin vein of tourmaline has a composition similar to the rim, but it is even more enriched in Na (0.79–0.84 *apfu*), Mg (2.40–2.49 *apfu*) and has the lowest content of Al (6.18–6.25 *apfu*). The calcium content is very low in the core and intermediate zone (<0.01 *apfu*), but increases at the rim and in vein dravite (0.05–0.12 *apfu*) (Fig. 3). Moreover, the vein tourmaline is enriched in F (0.11–0.17 *apfu*), whereas other zones except the intermediate zone (0.04–0.07 *apfu*) are generally F-poor, with up to 0.04 *apfu* (Table 1). The chemical zoning of dravite from Forshammar causes only slight changes in the lattice parameters: *a* 15.9252(7), *c* 7.1627(3) Å in the core (powder XRD data); *a* 15.9223(6), *c* 7.1706(5) Å in the rim according to powder XRD data, or *a* 15.921(1), *c* 7.175(1) Å from the crystal-structure refinement.

Variability in the chemical composition is the result of several substitutions, none of which is predominant. An increase of Al compared to an ideal composition of dravite (Fig. 4a) is driven by $Al^{X}\square Mg_{-1}Na_{-1}$ (Fig. 4c) and $AlOMg_{-1}(OH)_{-1}$ substitutions. The influence of $AlOMg_{-1}(OH)_{-1}$ substitution is manifested by a shift in composition from the ideal dravite – magnesio-foitite trend to "oxy-dravite" in the core, intermediate zone and rim; the dravite composition corresponds to the $Al^{X}\square Mg_{-1}Na_{-1}$ substitution trend only in the vein (Fig. 4b). However, the extent of the $AlOMg_{-1}(OH)_{-1}$ substitution is not sufficient to attain the composition of "oxy-dravite" (Fig. 4b). The excess of Al at the *Y* octahedra and also the lower Fe content result in a lower correlation of the $FeMg_{-1}$ substitution (Fig. 4d), which in contrast decrease the impact of the $Al^{X}\square Mg_{-1}Na_{-1}$ substitution in the intermediate zone (Fig. 4c). Slightly increased Ca contents concomitant with a decrease in

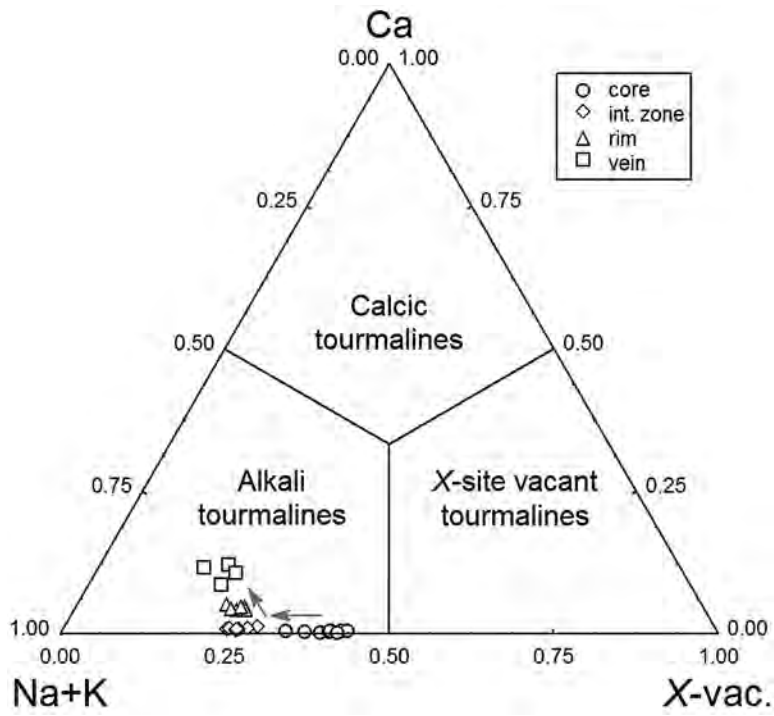

FIG. 3. Classification of dravite from the Forshammar pegmatite based on *X*-site occupancy (atomic proportions). Arrows indicate evolutional trend of dravite from core (o), through intermediate zone (◇), to rim (Δ) and vein (□).

^{Y,Z}Al in the rim and vein dravite (Table 1) indicate also a limited role of the uvite $^{X}Ca^{Z}Mg^{X}Na_{-1}{}^{Z}Al_{-1}$ substitution.

The crystal-structure refinement shows that the average <*T*–O> bond length, 1.6194(5) Å (Table 3), is within one standard deviation equivalent to a *T* site that is occupied only by Si (1.620 Å; see Ertl *et al.* 2010b). Hence there is no evidence for tetrahedrally coordinated B or Al. By using the correlation between Mg at the *Z* site and the average <*Z*–O> distance from Ertl *et al.* (2010a), which can be used for Fe-poor tourmalines, where the *Z* site is only occupied by Al and Mg, we can assign ~0.7 *apfu* Mg to the *Z* site of our tourmaline by using the <*Z*–O> distance, 1.923 Å (Table 4). By using the data acquired from the crystal-structure refinement and the chemical composition of the tourmaline rim (sample TSW an3; Table 2), we can propose the following formula: $\sim^{X}(Na_{0.7}Ca_{0.1}\square_{0.2})_{\Sigma 1}{}^{Y}(Mg_{1.5}Al_{1.2}Fe_{0.2}\square_{0.1})_{\Sigma 3}{}^{Z}(Al_{5.3}Mg_{0.7})_{\Sigma 6}(BO_3)_3(Si_6O_{18})(OH)_3[(OH),O]$. Hence this tourmaline shows a moderate Al–Mg disorder involving the *Y* and the *Z* site.

Most of trace elements were found to be below their detection limits; only Li, Ti, Mn Zn, Ga and the REE are significantly above the detection limits (Table 5). Zoning is also expressed in the distribution of trace elements. The contents of Ti, Mn, Y and REE are generally higher in the rim, whereas the contents of Zn, Ga and Sn decrease from the core to the rim (Table 5). Moreover, trace elements in the core display an oscillatory zoning that is not apparent in the major-element contents. Titanium, manganese and the REE accumulate on the contact of intermediate zone and rim and decrease toward the outer parts of the rim (Figs. 5a, b). The intermediate zone expresses a similar content of trace elements as the inner part of the rim, but it has the highest contents of Zn and Ga (Table 5).

The LA–ICP–MS data for the REE were normalized to chondritic values. All zones in tourmaline display a distinct enrichment in LREE, with Ce the most abundant in comparison to the HREE; La_N/Yb_N is in the range 32 – 464 (Fig. 6). The chondrite-normalized REE values regularly decrease with increasing atomic number; Ce_N shows a slight enrichment over La_N (Fig. 6). All zones of tourmaline display very strong negative Eu anomaly (Eu/Eu* = 0.005 to 0.05). The content of ΣREE increases from the core to the intermediate zone and the inner part of the rim, and then decreases to the outer part of the rim (Fig. 6).

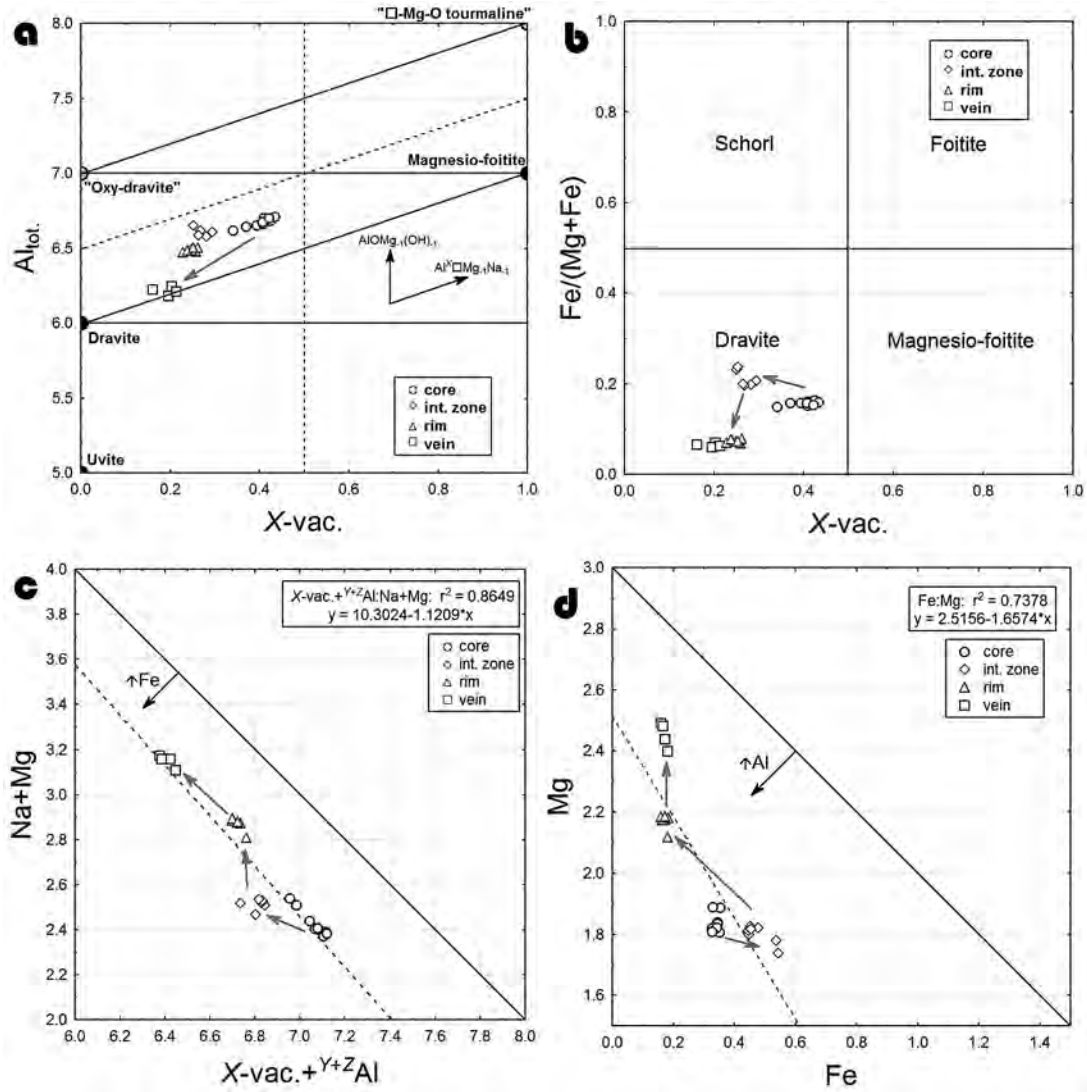

FIG. 4. Diagrams of tourmaline chemical composition (in *apfu*). a. Al_{total} *versus* $^{X}\square$ diagram. b. Fe/(Mg + Fe) *versus* $^{X}\square$ diagram. c. Na + Mg *versus* $^{X}\square+^{Y+Z}Al$ diagram. d. Mg *versus* Fe diagram. Gray arrows represent change of chemical composition within tourmaline zones. Black arrows represent substitution vectors (a) or trends of cation increase (c, d). Solid line represent ideal substitution trends (a, c, d) or borders of mineral composition (b). Dashed lines represent borders of mineral composition (a) or correlation trend-line of analyzed samples (c, d).

Associated minerals

Dravite from the Forshammar pegmatite contains thin veinlets and inclusions of other minerals. Muscovite occur in veinlets cutting tourmaline crystals (Figs. 2a, b); it has higher content of Mg than Fe, an atomic Fe/(Fe+Mg) value in the range 0.07–0.10, which is similar to the host tourmaline (Table 6). Zircon and xenotime-(Y) occur as tiny euhedral inclusions (usually 50 to 150 μm across) in dravite (Fig. 7). The zircon is Hf-rich (3.6 to 6.3 wt.% HfO_2, 0.03–0.06 *apfu* Hf, $Zr/Hf_{wt.}$ = 6.9 to 12.2). The content of Y+REE is relatively low (0.01–0.03 *apfu*); some crystals are slightly enriched in U (up to 1.5 wt.% UO_2, 0.011 *apfu*; Table 7). Irregular zoning and fractures in zircon could indicate (partial) metamictization. Moreover, zircon contains numerous

tiny inclusions of xenotime-(Y) (Fig. 7). Xenotime-(Y) shows a high atomic Y/(Y+REE) value (0.80), 0.19 *apfu* ΣREE; Dy (0.043 *apfu*) and Yb (0.048 *apfu*) are the most abundant REE (Table 7). Hydroxylbastnäsite-(Ce) forms tiny veinlets or irregular fillings (up to ~300 μm across) with muscovite in host dravite or at the tourmaline–quartz boundary (Fig. 2). It shows a relatively homogeneous composition, with a distinct dominance of Ce over the other REE, negligible contents of Th, U (both <0.01 *apfu*), and a low F concentration (~0.25 *apfu*) (Table 8).

The chondrite normalization of the REE in accessory minerals was only possible from the electron-microprobe data, as their minute size did not allow for LA–ICP–MS analysis. Hydroxylbastnäsite-(Ce) is distinctly enriched in LREE (Fig. 8a), whereas xenotime-(Y) is enriched in HREE; both of them display a strong negative Eu anomaly (Fig. 8b).

Discussion and Conclusions

Crystal chemistry of tourmaline

As suggested by our EMPA and LA–ICP–MS data, the Forshammar tourmaline shows relatively minor chemical variability. It is controlled by substitutions of major cations including Al, Mg and Na; other cations play only negligible roles in the observed crystallochemical variations. Our tourmaline has a poor correlation of $FeMg_{-1}$ substitution; its deviation from the ideal trend is due to a low Fe content.

TABLE 5. CONTENTS OF TRACE ELEMENTS IN TOURMALINE FROM FORSHAMMAR

	d.l.	core	int. zone	rim
Li	170	b.d.l. - 220	240	b.d.l. - 369
Ti	8	380 - 814	1127	933 -1611
Mn	1	206 - 406	635	207 - 977
Co	0.1	0.1 - 1.5	0.5	0.60 - 1.4
Zn	0.8	34 - 84	86	16 - 37
Ga	0.4	58 - 115	105	54 - 86
Y	0.10	0.60 - 1.7	5.1	1.3 - 6.9
Sn	1.2	1.9 - 9.8	6.6	2.4 - 5.6
La	0.1	15 - 30	155	44 - 210
Ce	0.1	53 - 108	548	112 - 670
Pr	0.06	7.4 - 14	63	14 - 79
Nd	0.1	27 - 58	190	45 - 251
Sm	0.2	3.5 - 9.0	28	5.9 - 30
Eu	0.01	b.d.l. - 0.07	b.d.l.	0.02 - 0.15
Gd	0.2	1.3 - 3.4	13	2.8 - 11
Tb	0.01	0.09 - 0.32	0.77	0.16 - 0.81
Dy	0.01	0.19 - 0.72	2.2	0.43 - 2.5
Ho	0.01	b.d.l. - 0.05	0.14	b.d.l. - 0.24
Er	0.01	0.03 - 0.29	0.27	0.05 - 0.43
Tm	0.01	b.d.l. - 0.03	b.d.l.	b.d.l. - 0.04
Yb	0.01	0.06 - 0.47	0.33	0.10 - 0.38

These data, expressed in ppm, were acquired by laser-ablation inductively coupled plasma – mass spectrometry (LA–ICP–MS). Notations: d.l.: detection limit, b.d.l.: below detection limit.

The occupancy of *Y* and *Z* sites is mainly controlled by exchange of Al and Mg. Their distribution over octahedral sites in dravitic to olenitic tourmalines reflects their disorder (Hawthorne *et al*. 1993, Ertl *et al*. 2008, 2010a, Bosi *et al*. 2010). Our tourmaline exhibits Al–Mg disorder involving the *Y* and the *Z* sites, but it is not sufficient to change the composition from dravite to olenite. Charge-balance requirements of the substitution of Al^{3+} for Mg^{2+} are partly satisfied by an alkali decrease (mainly in the core, decreasing to the rim), but the excess of Al in comparison to the proportion of *X*-site vacancy suggests a deprotonization of ^{V+W}OH. The observed variation in chemical composition in the *Y* site with increased content of $^{Y}Al^{3+}$, which is observable in dravite from Forshammar ($^{Y}Al^{3+}$ in the range 0.18–0.71 *apfu* from the ordered formula; $^{Y}Al^{3+}$ = 1.2 *apfu* in the structural formula) is typical of the dravite to "oxy-dravite" trend (Bloodaxe *et al*. 1999, Bosi & Lucchesi 2004, Novák *et al*. 2004). The proportion of ^{V+W}O calculated from a charge-balanced formula is not sufficiently accurate, and data from the structural

TABLE 6. REPRESENTATIVE COMPOSITIONS OF MUSCOVITE FROM FORSHAMMAR, BERGSLAGEN PROVINCE, SWEDEN

	TSW an3	TSW an4	TSW an5	TSW an8	TSW an9
SiO_2 wt.%	50.52	50.28	47.68	49.13	48.88
TiO_2	0.10	0.12	0.12	0.04	0.04
Al_2O_3	30.59	29.92	34.22	34.33	35.20
FeO	0.47	0.48	0.25	0.22	0.17
MgO	2.80	2.99	1.33	1.55	1.07
CaO	0.03	0.06	0.04	0.06	0.06
Na_2O	0.09	0.20	0.12	0.13	0.10
K_2O	10.94	10.61	10.73	10.49	9.93
H_2O*	4.55	4.49	4.50	4.59	4.59
Cl	0.02	0.07	0.01	0.01	b.d.l.
sum	100.10	99.25	99.05	100.58	100.08
O=Cl	-0.01	-0.03	0.00	0.00	0.00
Total	100.09	99.21	99.05	100.58	100.08
Si^{4+} *apfu*	3.328	3.341	3.173	3.209	3.194
$^{IV}Al^{3+}$	0.672	0.659	0.827	0.791	0.806
Σ*T*	4.000	4.000	4.000	4.000	4.000
Ti^{4+}	0.005	0.006	0.006	0.002	0.002
$^{VI}Al^{3+}$	1.703	1.684	1.857	1.852	1.906
Fe^{2+}	0.026	0.027	0.014	0.012	0.009
Mg^{2+}	0.275	0.296	0.132	0.151	0.104
Σ*M*	2.009	2.013	2.009	2.016	2.021
Ca^{2+}	0.002	0.005	0.003	0.004	0.004
Na^{+}	0.011	0.026	0.016	0.017	0.013
K^{+}	0.920	0.899	0.911	0.874	0.828
□	0.067	0.070	0.071	0.105	0.155
Σ*I*	0.933	0.930	0.929	0.895	0.845
Cl^{-}	0.002	0.008	0.001	0.001	-
OH^{-}	1.998	1.992	1.999	1.999	2.000
Fe/(Fe + Mg)	0.09	0.08	0.10	0.07	0.08

The analytical data, acquired with an electron microprobe, are first reported in wt.%, and then converted to atoms per formula unit on the basis of 10O + 2(OH) anions per formula unit. A component is not considered significant unless its value exceeds the uncertainty (b.d.l.: below detection limit). * H_2O was calculated assuming OH + Cl = 2 *apfu*.

formula do not take any local inhomogeneities into account. However, the calculated $^{V+W}$O along with dravite to "oxy-dravite" trend (Fig. 4a) are good indicators that the $AlOMg_{-1}(OH)_{-1}$ substitution is the most likely mechanism to balance the local excess in charge (Medaris *et al.* 2003). Thus, if O dominates the *W* site in the ordered formula, some compositions of tourmaline from Forshammar could be classified as "oxy-dravite" according to Henry *et al.* (2011).

The distribution of the REE and other trace elements

Dravite from the Forshammar pegmatite is markedly enriched in the REE in comparison to all known tourmalines from granitic pegmatites (Neiva 1974, Jolliff *et al.* 1987, Hellingwerf *et al.* 1994, Roda *et al.* 1995, Jiang *et al.* 1997, Roda-Robles *et al.* 2004, Ertl *et al.* 2006, Novák *et al.* 2011). In particular, the rim zones attain up to ~1200 ppm ΣREE, ≤210 ppm La, ≤670 ppm Ce, ≤250 ppm Nd, ≤30 ppm Sm (Tables 5, 6). A careful inspection of each area of the tourmaline grain before LA–ICP–MS measurement and the general enrichment in REE in all analyzed spots minimize the possible influence of tiny inclusions of hydroxylbastnäsite-(Ce) on the analytical results.

It seems likely that the REE occupy the *X* site of the tourmaline structure. Tourmaline with dominant Na^+ and Ca^{2+} cations at the *X* site prefers LREE with larger ionic radii rather than HREE and Y. The ionic radius of 9-coordinated Na^+ cation is 1.24 Å, similar to $^{[9]}Ca^{2+}$ (1.18 Å) and La^{3+} to Sm^{3+} in the same coordination (1.216 to 1.132 Å), whereas the ionic radius of the following HREE decrease down to 1.032 Å for $^{[9]}Lu^{3+}$ (Shannon 1976). The relationship of Ca and REE is also pronounced in tourmaline from Forshammar; the highest content of REE is in the rim and veins, which are also the most enriched in Ca.

The REE content of tourmaline in granitic pegmatites is generally low; usually ΣREE is below ~20 ppm (La and Ce <10 ppm), with wide variations of La_N/Yb_N (0.16 to 433) and Eu/Eu* (0.03 to over 1) (Table 5). Only a few pegmatite populations include tourmaline remarkably enriched in the REE (Table 9), *e.g.*, elbaite from Nuristan, Afghanistan and Anjanabonoina, Madagascar (Ertl *et al.* 2006) or dravite to schorl from the Třebíč pluton, Czech Republic (Novák *et al.* 2011). The Forshammar dravite also show a high La_N/Yb_N value (32 to 464) and a strikingly negative Eu anomaly (Eu/Eu* = 0.005 to 0.05) in comparison to other known tourmalines from granitic pegmatites (Table 6). A strong negative Eu anomaly in tourmaline and also in xenotime-(Y) and hydroxylbastnäsite-(Ce) suggests low oxygen fugacity or some degree of magmatic fractionation of the host rock (*e.g.*, Möller & Muecke 1984), which is a characteristic feature of granitic pegmatites. However, some features of Forshammar tourmaline, including the high X_{Mg} value, suggest a low degree of fractionation of pegmatite.

The REE concentration in tourmalines from granitic rocks also is generally low (usually <20 ppm La and Ce), with LREE > HREE and a negative Eu anomaly (Bea 1996, Jiang *et al.* 1997, Pesquera *et al.* 2005). Yet, it is noteworthy that a tourmaline from an unspecified pegmatite in the Riddarhyttan area, near Forshammar in central Bergslagen, also attains elevated REE contents, as measured by neutron-activation analysis (Hellingwerf *et al.* 1994). Variable but commonly higher REE contents are characteristic of tourmaline in tourmalinites, gneisses, and metasediments, commonly spatially related to metamorphic, magmatic or hydrothermal ore deposits, where dominant La and Ce locally attain up to ~130 and 280 ppm, respectively (Hellingwerf *et al.* 1994, Torres-Ruiz *et al.* 2003, Pesquera *et al.* 2005, Garda *et al.* 2010, Klemme *et al.* 2011). The tourmaline in tourmaline–quartz veins is usually very poor in REE (<20 ppm La, Ce; <50 ppm ΣREE; *e.g.*, King *et al.* 1988, Yavuz *et al.* 1999, Jiang *et al.* 1999,

TABLE 7. REPRESENTATIVE COMPOSITIONS OF ZIRCON AND XENOTIME-(Y) FROM FORSHAMMAR, BERGSLAGEN PROVINCE, SWEDEN

	Zrn TSW-2	Zrn TSW-5	Xnt TSW-1		Zrn TSW-2	Zrn TSW-5	Xnt TSW-1
P_2O_5 wt.%	0.11	2.03	36.46	P *apfu*	0.003	0.056	0.996
As_2O_5	0.14	0.19	b.d.l.	As	0.002	0.003	-
SiO_2	31.67	28.76	0.12	Si	0.992	0.939	0.004
TiO_2	0.04	0.05	b.d.l.	Ti	0.001	0.001	-
ZrO_2	61.22	49.83	0.13	Al	0.001	-	-
HfO_2	4.61	6.32	0.10	Σ*B*	0.999	0.999	1.000
ThO_2	b.d.l.	b.d.l.	0.09				
UO_2	0.10	0.52	0.09	Zr	0.935	0.794	0.002
Al_2O_3	0.04	b.d.l.	b.d.l.	Hf	0.041	0.059	0.001
Y_2O_3	0.11	4.47	45.19	Th	-	-	0.001
La_2O_3	b.d.l.	b.d.l.	b.d.l.	U	0.001	0.004	0.001
Ce_2O_3	0.04	0.07	0.07	Y	0.002	0.078	0.776
Pr_2O_3	0.13	0.13	0.16	La	-	-	-
Nd_2O_3	b.d.l.	b.d.l.	0.08	Ce	0.001	0.001	0.001
Sm_2O_3	b.d.l.	b.d.l.	0.60	Pr	0.001	0.002	0.002
Eu_2O_3	0.12	0.16	b.d.l.	Nd	-	-	0.001
Gd_2O_3	0.12	0.15	2.43	Sm	-	-	0.007
Tb_2O_3	b.d.l.	b.d.l.	0.55	Eu	0.001	0.002	-
Dy_2O_3	0.04	0.29	4.15	Gd	0.001	0.002	0.026
Ho_2O_3	b.d.l.	b.d.l.	0.68	Tb	-	-	0.006
Er_2O_3	0.31	0.80	3.46	Dy	0.001	0.003	0.043
Tm_2O_3	0.10	0.22	0.67	Ho	-	-	0.007
Yb_2O_3	0.21	1.64	4.85	Er	0.003	0.008	0.035
Lu_2O_3	b.d.l.	0.36	0.76	Tm	0.001	0.002	0.007
FeO	0.18	0.74	0.09	Yb	0.002	0.016	0.048
CaO	0.08	1.33	b.d.l.	Lu	-	0.004	0.007
SrO	0.08	0.09	b.d.l.	Fe	0.004	0.018	0.002
				Ca	0.003	0.047	-
Total	99.45	98.15	100.73	Sr	0.001	0.002	-
				Σ*A*	0.996	1.042	0.973
				Σ cations	1.995	2.041	1.973
				Y+REE	0.011	0.118	0.966
				Y/(Y+REE)	0.18	0.66	0.80
				Zr/Hf wt.	11.59	6.88	

The analytical data, acquired with an electron microprobe, are first reported in wt.%, and then converted to atoms per formula unit on the basis of P + As + Si + Ti + Al = 1 *apfu*. A component is not considered significant unless its value exceeds the uncertainty (b.d.l.: below detection limit). Symbols used: Zrn: zircon, Xnt: xenotime-(Y).

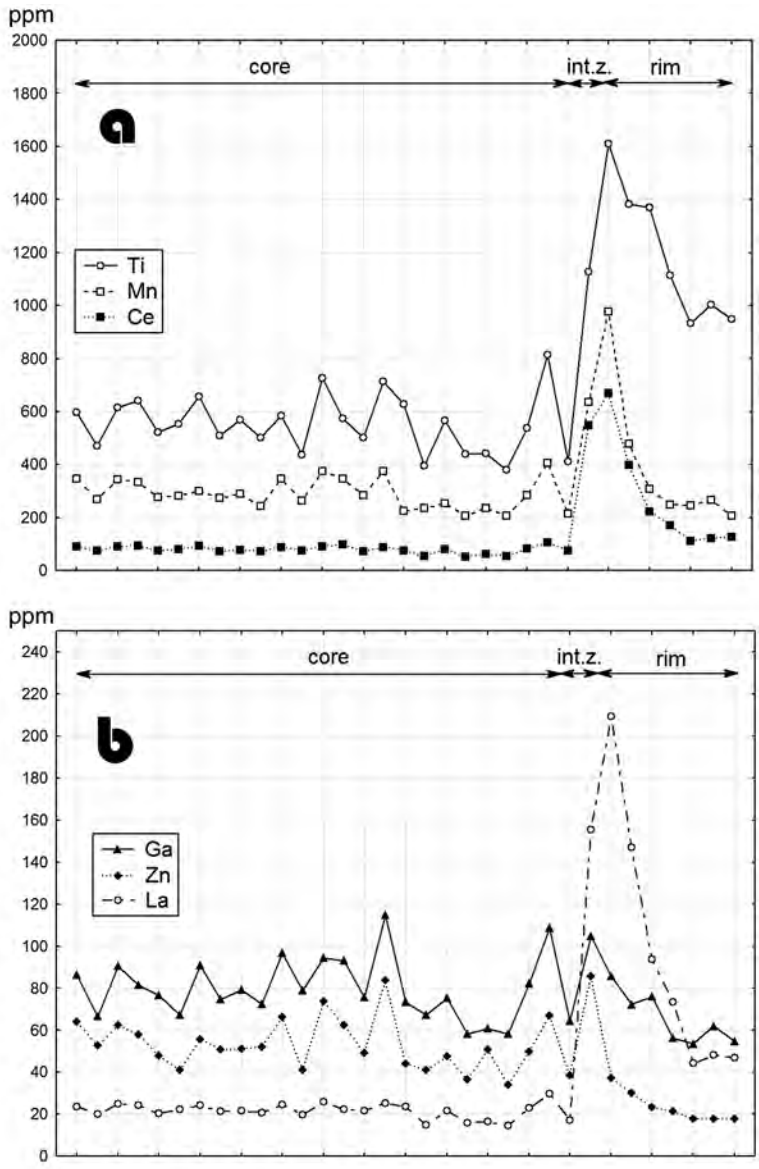

FIG. 5. Cross-section diagrams of trace elements in dravite from the Forshammar pegmatite. The distance between tickmarks on the X axis represents *ca.* 100 μm on the real sample.

2004, Deksissa & Koeberl 2002, Roberts *et al.* 2006). However, the highest REE concentrations observed in tourmaline were reported from veins, also from the Bergslagen ore province in central Sweden (up to 783 ppm La and 1560 ppm Ce; Hellingwerf *et al.* 1994). These highest reported contents of REE in various genetic types of tourmaline (pegmatites, metamorphic rocks, quartz veins) from same general part of the Bergslagen province indicate an important role of regional lithology on the trace-element (at least REE) concentrations in this mineral group.

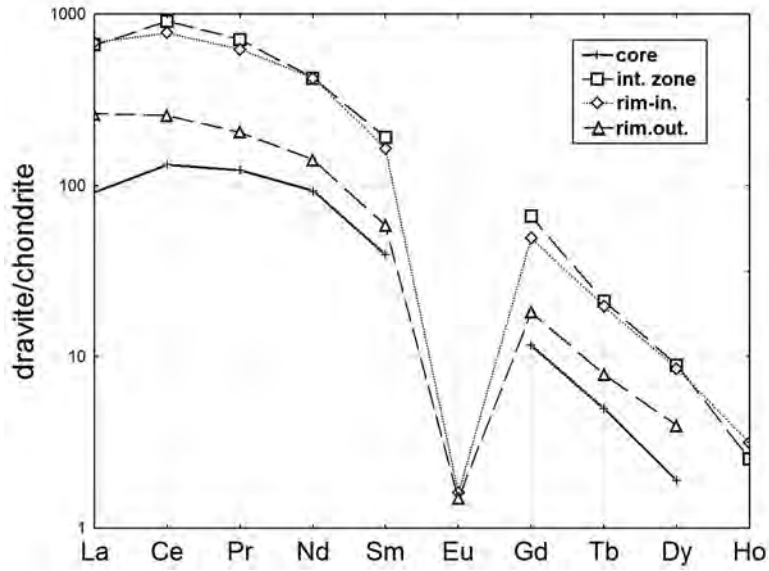

FIG. 6. Average chondrite-normalized REE patterns of several zones in dravite from the Forshammar pegmatite. Chondrite values from Anders & Grevesse (1989).

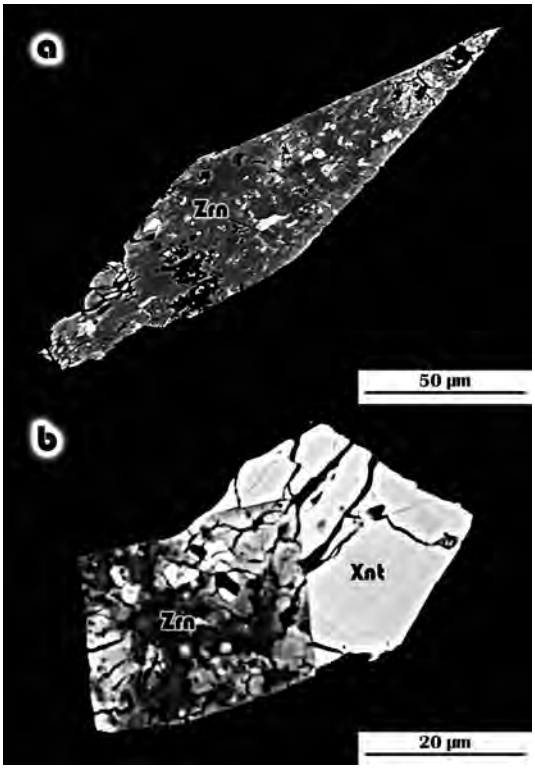

The tourmaline rim with the highest REE concentrations may also have been influenced or may be the result of a later hydrothermal process that could mobilize the rare earths. The mobilization of the REE is also suggested by formation of hydroxylbastnäsite-(Ce) at a late stage of this hydrothermal process. The behavior of the REE is usually controlled by F (Gramaccioli *et al.* 1999). However, the low content of F in tourmaline and muscovite and the presence of hydroxylbastnäsite-(Ce) in spite of more common bastnäsite-(Ce) suggest only a negligible role of F. Thus, the enrichment in REE in tourmaline from Forshammar could be likely controlled by the activity of CO_2.

Concentrations of Co and Ga (0.1 to 1.5 and 54 to 115 ppm, respectively; Table 5) are similar, Y (0.6 to 6.9 ppm) reveals higher contents, whereas Zn and Sn (16 to 86 and 1.9 to 9.8 ppm, respectively) show usually lower contents compared to the trace-element concentrations reported from tourmalines in pegmatites (Neiva 1974, Hellingwerf *et al.* 1994, Roda *et al.* 1995, Jiang *et al.*

FIG. 7. BSE photomicrographs of zircon (a) and zircon – xenotime-(Y) inclusions (b) in dravite from the Forshammar pegmatite. Note the tiny anhedral inclusions of xenotime-(Y) in zircon. Symbols: Zrn: zircon, Xnt: xenotime-(Y).

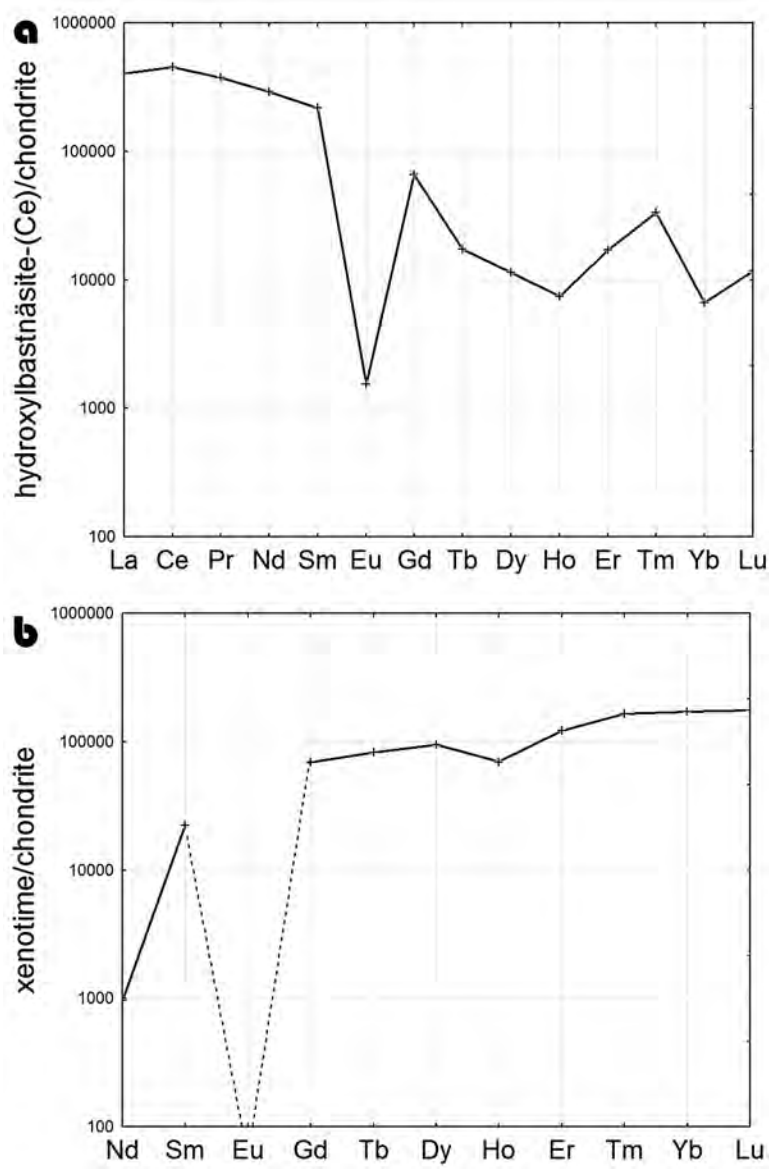

FIG. 8. Average chondrite-normalized REE patterns of a) hydroxylbastnäsite-(Ce) and b) xenotime-(Y) occurring as accessory minerals in tourmaline from Forshammar. Chondrite values from Anders & Grevesse (1989).

1997, Keller *et al*. 1999, Roda-Robles *et al*. 2004, Ertl *et al*. 2006, Novák *et al*. 2011).

The evolution of tourmaline

The observed zoning in the dravite suggests at least two different processes in the growth of tourmaline. This is suggested by the chemical composition of the core, which differs from other zones in some features. The core has a lower Ca content and distinctly higher *X*-site vacancy (Table 1) in comparison to other zones. Slight oscillatory zoning apparent in the trace-element distribution suggests that the core is likely the product of a magmatic process. The X_{Mg} value of the rim (0.76)

is similar to that in tourmaline from unusual NYF pegmatites in Třebíč pluton, Czech Republic (up to 0.8; Novák *et al*. 2011). However, dravite from Forshammar has distinctly higher Al content (6.6 – 6.7 *apfu*) and *X*-site vacancy (0.3 – 0.4) than tourmalines from the Třebíč pluton, with up to 5.7 Al *apfu* and 0.15 of *X*-site vacancy (Novák *et al*. 2011).

The intermediate zone and rim display increasing Ca and Ti contents and a decreasing proportion of *X*-site vacancy compared to the core. It could indicate prograde *P–T* conditions during high-grade metamorphism (Henry & Dutrow 1996). However, on the basis of presently available data and observations, the central Swedish pegmatites formed around 1.8 Ga are unlikely to have experienced any significant overprinting geological event other than brittle deformation. The fact that the granitic pegmatites in the Forshammar area are dominated by a graphic K-feldspar – quartz intergrowth, as well as being unzoned or only marginally so around small, local core pods of quartz, tends to indicate rapid formation from a quickly cooled system. The geochemistry may be an effect of their localized occurrence within a terrane dominated by felsic metavolcanic rock, rather than within metasedimentary units (*e.g.,* Smeds 1990). The lack of tetrahedrally coordinated Al, which usually occurs in significant amounts in tourmaline from higher-grade lithologies (Henry & Dutrow 1996), suggests that the rim of Forshammar tourmaline is not a product of a later metamorphic event. However, it is likely that it grew during a later hydrothermal stage or stages of pegmatite evolution. We can assume that the hydrothermal fluid, which formed intermediate zone, was enriched in Fe, Ca and trace elements including Ti, Mn and REE compared to the rim. The content of Ca and Ti decreases from the contact of the intermediate zone and rim to the outer part of the rim, which could suggest a decrease in the temperature (Henry & Dutrow 1996). A similar trend of enrichment in Ca and Ti was also observed in part of tourmalines in pegmatites from the Třebíč pluton, which suggests an early subsolidus origin (Novák *et al*. 2011). The decrease in Fe, Mn and REE content from core to the rim can be most likely explained by the change of the fluid composition during the formation of the rim. The increased and variable content of REE may indicate a contribution of magmatic–hydrothermal fluids (Garda *et al*. 2010), and it supports the assumption of subsolidus, most likely hydrothermal origin for the intermediate zone and rim of the Forshammar tourmaline. The crystallization of tourmaline ended with the veinlets of tourmaline, which have even lower Al and higher Mg contents than the rim. Even younger hydroxylbastnäsite-(Ce) and muscovite are apparently the products of the final stage or a later hydrothermal process.

TABLE 8. REPRESENTATIVE COMPOSITIONS OF HYDROXYLBASTNÄSITE-(Ce) FROM FORSHAMMAR, BERGSLAGEN PROVINCE, SWEDEN

	TSW51	TSW52		TSW51	TSW52
CO_2 * wt.%	18.80	18.63	C *apfu*	0.997	0.995
SiO_2	0.09	0.14	Si	0.003	0.005
ThO_2	b.d.l.	0.04	Σ*B*	1.000	1.000
UO_2	0.06	0.05			
Y_2O_3	0.79	1.21	Th	-	0.001
La_2O_3	11.96	10.69	U	0.001	0.001
Ce_2O_3	32.41	30.71	Y	0.016	0.025
Pr_2O_3	3.82	3.90	La	0.171	0.154
Nd_2O_3	15.19	15.85	Ce	0.461	0.440
Sm_2O_3	3.63	4.06	Pr	0.054	0.056
Eu_2O_3	b.d.l.	0.04	Nd	0.211	0.221
Gd_2O_3	1.39	1.83	Sm	0.049	0.055
Tb_2O_3	0.10	b.d.l.	Eu	-	0.001
Dy_2O_3	0.28	0.43	Gd	0.018	0.024
Ho_2O_3	0.12	0.07	Tb	0.001	-
Er_2O_3	0.26	0.34	Dy	0.004	0.005
Tm_2O_3	0.12	0.09	Ho	0.001	0.001
Yb_2O_3	0.17	0.13	Er	0.003	0.004
Lu_2O_3	b.d.l.	b.d.l.	Tm	0.001	0.001
FeO	0.07	b.d.l.	Yb	0.002	0.002
MnO	b.d.l.	0.04	Lu	-	-
CaO	0.04	0.07	Fe	0.002	-
SrO	b.d.l.	0.06	Mn	-	0.001
H_2O**	2.90	2.82	Ca	0.002	0.003
F	2.01	2.11	Sr	-	0.001
Cl	0.04	0.04	Σ*A*	0.997	0.994
O=F	-0.85	-0.89	ΣREE+Y	0.992	0.989
O=Cl	-0.01	-0.01	Σ cations	1.997	1.994
Total	93.39	92.45	OH	0.751	0.736
			F	0.247	0.261
			Cl	0.003	0.003
			Σ*X*	1.001	1.000
			O	3.000	3.000
			F/(F+OH)	0.25	0.26
			100Ce/(REE+Y)	46.5	44.5
			100LREE/(REE+Y)	95.4	93.7

The analytical data, acquired with an electron microprobe, are first reported in wt.%, and then converted to atoms per formula unit on the basis of 4 anions. * C + Si = 1 *apfu*. ** OH + F + Cl = 1 *apfu*. A component is not considered significant unless its value exceeds the uncertainty (b.d.l.: below detection limit).

Acknowledgements

This contribution is dedicated to Professor Petr Černý, University of Manitoba, an eminent mineralogist whose contribution to research on granitic pegmatites, their minerals and genesis is outstanding and influential. We thank Jarek Majka, Jaroslav Pršek and Peter Chudík for their helping hands in the field research and sample collecting. We also thank Daniel Ozdín for assistance with the EMPA analysis. We are indebted to Milan Novák and Robert F. Martin for editorial handling and Darrell J. Henry and Hartmut Beurlen for their detailed reviews and very useful suggestions. This work was supported by the Slovak Research and Development Agency under contracts VVCE–0033–07, APVV–0557–06 (to PB and PU) and by the Austrian Science Fund (FWF) project no. P23012–N19 (to AE).

TABLE 9. COMPARISON OF REE CONTENTS IN TOURMALINES FROM PEGMATITE AT SELECTED LOCALITIES

Locality	La (ppm)	Ce (ppm)	Yb (ppm)	La_N/Yb_N	Eu/Eu*	Mineral	Reference
Alijó-Sanfins area, Portugal	<0.2 – 3.9	<0.3 – 0.9	n.d.	n.d.	n.d.	schorl	Neiva (1974)
Fregeneda area, Spain	0.4 – 1.0	3.4	0.1 – 0.7	1.0 – 7.1	>1	schorl to dravite	Roda *et al*. (1995)
Bob Ingersoll, U.S.A.	0.05 – 1.8	0.02 – 3.6	0.001 – 0.25	4.9 – 58	<0.47 – >1	schorl to elbaite	Jolliff *et al*. (1987)
Eastern Liaoning, P. R. China	2.4	4.4	0.12	14	5.9	schorl to dravite	Jiang *et al*. (1997)
Stoffhütte, Austria	3.5	8.3	0.24	10	0.28	olenite	Ertl *et al*. (2006)
Nuristan, Afghanistan	13	47	0.02	433	0.03	elbaite	Ertl *et al*. (2006)
Anjanabonoina, Madagascar	47	71	0.09	359	0.46	elbaite	Ertl *et al*. (2006)
Třebíč pluton, Czech Republic	6.2 – 51	7.6 – 63	n.d.	n.d.	n.d.	dravite to schorl	Novák *et al*. (2011)
Bergslagen area, Sweden	0.8 – 35	2.8 – 83	0.3 – 5.0	0.16 – 14	<1	schorl to dravite	Hellingwerf *et al*. (1994)
Forshammar, Sweden	14.0 – 210	55.0 – 670	0.06 – 0.38	32.0 – 464	0.005 – 0.05	dravite	this study

n.d.: not determined.

References

Ambros, M. (1983): Beskrivning till berggrundskartan 1:50 000 – VIF Lindesberg NO (description to the map of solid rocks Lindesberg NO). *Sveriges Geologiska Undersökning Af* 141, 75 pp. + map.

Anders, E. & Grevesse, N. (1989): Abundances of the elements: meteoritic and solar. *Geochim. Cosmochim. Acta* **53**, 197-214.

Bea, F. (1996): Residence of REE, Y, Th and U in granites and crustal protoliths; implications for the chemistry of crustal melts. *J. Petrol.* **37**, 521-552.

Bernard, J.H. & Hyršl, J. (2006): *Minerals and their Localities* (2nd ed.). Granit, Prague, Czech Republic.

Bloodaxe, E.S., Hughes, J.M., Dyar, M.D., Grew, E.S. & Guidotti, C.V. (1999): Linking structure and chemistry in the schorl–dravite series. *Am. Mineral.* **84**, 922-928.

Bosi, F., Balić-Žunić, T. & Surour A.A. (2010): Crystal structure analyses of four tourmaline specimens from the Cleopatra's mines (Egypt) and Jabal Zalm (Saudi Arabia), and the role of Al in the tourmaline group. *Am. Mineral.* **95**, 510-518.

Bosi, F. & Lucchesi, S. (2004): Crystal chemistry of the schorl–dravite series. *Eur. J. Mineral.* **16**, 335-344.

Brotzen, O. (1959): Mineral-association in granitic pegmatites. A statistical study. *Geol. Fören. Stockholm Förh.* **81**, 231-296.

Bruker (2010a): DIFFRACplus EVA. http://www.brukeraxs.com/eva.html

Bruker (2010b): DIFFRACplus TOPAS. http://www.brukeraxs.de/topas.html

Deksissa, D.J. & Koeberl, C. (2002): Geochemistry and petrography of gold – quartz – tourmaline veins of the Okote area, southern Ethiopia: implications for gold exploration. *Mineral. Petrol.* **75**, 101-122.

Ertl, A., Hughes, J.M., Prowatke, S., Ludwig, T., Prasad, P.S.R., Brandstätter, F., Körner, W., Schuster, R., Pertlik, F. & Marschall, H. (2006): Tetrahedrally coordinated boron in tourmalines from the liddicoatite–elbaite series from Madagascar: structure, chemistry, and infrared spectroscopic studies. *Am. Mineral.* **91**, 1847-1856.

Ertl, A., Mali, H., Schuster, R., Körner, W., Hughes, J.M., Brandstätter, F. & Tillmanns, E. (2010a): Li-bearing, disordered Mg-rich tourmaline from a pegmatite–marble contact in the Austroalpine basement units (Styria, Austria). *Mineral. Petrol.* **99**, 89-104.

Ertl, A., Marschall, H.R., Giester, G., Henry, D.J., Schertl, H.-P., Ntaflos, T., Luvizotto, G.L., Nasdala, L. & Tillmanns, E. (2010b): Metamorphic ultra high-pressure tourmaline: structure, chemistry, and correlations to P–T conditions. *Am. Mineral.* **95**, 1-10.

Ertl, A., Rossman, G.R., Hughes J.M., Ma, Chi & Brandstätter, F. (2008) V^{3+}-bearing, Mg-rich, strongly disordered olenite from a graphite deposit near Amstall, Lower Austria: a structural, chemical and spectroscopic investigation. *Neues Jahrb. Mineral., Abh.* **184**, 243-253.

FISCHER, R.X. & TILLMANNS, E. (1988): The equivalent isotropic displacement factor. *Acta Crystallogr.* **C44**, 775-776.

FLINK, G. (1917): Bidrag till Sveriges mineralogi. IV. 112. Andalusit. *Arkiv Kemi, Mineral. Geol.* **6**, 72-74.

GARDA, G.M., BELJAVSKIS, P., D'AGOSTINO, L.Z. & WIEDENBECK, M. (2010): Tourmaline and rutile as indicators of a magmatic–hydrothermal origin for tourmalinite layers in the São José do Barreiro area, NE Ribeira Belt, southern Brazil. *Geol. USP Sér. Cient.* **10**(3), 97-117.

GRAMACCIOLI, C. M., DIELLA, V. & DEMARTIN, F. (1999): The role of fluoride complexes in REE geochemistry and the importance of 4f electrons: some examples in minerals. *Eur. J. Mineral.* **11**, 983-992.

HAWTHORNE, F.C., MACDONALD, D.J. & BURNS, P.C. (1993): Reassignment of cation site occupancies in tourmaline: Al–Mg disorder in the crystal structure of dravite. *Am. Mineral.* **78**, 265-270.

HELLINGWERF, R.H., GATEDAL, K., GALLAGHER, V. & BAKER, J.H. (1994): Tourmaline in the central Swedish ore district. *Mineral. Deposita* **29**, 189-205.

HENRY, D.J. & DUTROW, B.L. (1996): Metamorphic tourmaline and its petrologic applications. *In* Boron: Mineralogy, Petrology and Geochemistry (E.S. Grew & L.M. Anovitz, eds.). *Rev. Mineral.* **33**, 503-557.

HENRY, D.J., NOVÁK, M., HAWTHORNE, F.C., ERTL, A., DUTROW, B.L., UHER, P. & PEZZOTTA, F. (2011): Nomenclature of the tourmaline supergroup-minerals. *Am. Mineral.* **96**, 895-913.

IVARSSON, C. & JOHANSSON, Å. (1995): U–Pb zircon dating of Stockholm granite at Frescati. *Geol. Fören. Stockholm Förh.* **117**, 67-68.

JIANG SHAO-YONG, HAN FA, SHEN JIAN-ZHONG & PALMER M.R. (1999): Chemical and Rb–Sr, Sm–Nd isotopic systematics of tourmaline from the Dachang Sn-polymetallic ore deposit, Guangxi Province, P.R. China. *Chem. Geol.* **157**, 49-67.

JIANG SHAO-YONG, PALMER, M.R., PENG QI-MING & YANG JING-HONG (1997): Chemical and stable isotopic compositions of Proterozoic metamorphosed evaporites and associated tourmalines from the Houxianyu borate deposit, eastern Liaoning, China. *Chem. Geol.* **135**, 189-211.

JIANG SHAO-YONG, YU JI-MIN & LU JIAN-JUN (2004): Trace and rare-earth element geochemistry in tourmaline and cassiterite from the Yunlong tin deposit, Yunnan, China: implication for migmatitic–hydrothermal fluid evolution and ore genesis. *Chem. Geol.* **209**, 193-213.

JOLLIFF, B.L., PAPIKE, J.J. & LAUL, J.C. (1987): Mineral recorders of pegmatite internal evolution: REE contents of tourmaline from the Bob Ingersoll pegmatite, South Dakota. *Geochim. Cosmochim. Acta* **51**, 2225-2232.

KELLER, P., RODA ROBLES, E., PESQUERA PÉREZ, A. & FONTAN, F. (1999): Chemistry, paragenesis and significance of tourmaline in pegmatites of the Southern Tin Belt, central Namibia. *Chem. Geol.* **158**, 203-225.

KING, R.W., KERRICH, R.W. & DADDAR, R. (1988): REE distributions in tourmaline: an INAA technique involving pretreatment by B volatilization *Am. Mineral.* **73**, 424-431.

KLEMME, S., MARSCHALL, H.R., JACOB, D.E., PROWATKE, S. & LUDWIG, T. (2011): Trace-element partitioning and boron isotope fractionation between white mica and tourmaline. *Can. Mineral.* **49**, 165-176.

LONDON, D. (2008): *Pegmatites*. The Canadian Mineralogist, Special Publication **10**.

LUNDEGÅRDH, P.H. (1971): *Nyttosten i Sverige*. Almqvist & Wiksell, Stockholm, Sweden.

LUNDSTRÖM, I., ALLEN, R.L., PERSSON, P.-O. & RIPA, M. (1998): Stratigraphies and depositional ages of Svecofennian, Palaeoproterozoic metavolcanic rocks in E. Svealand and Bergslagen, south central Sweden. *Geol. Fören. Stockholm Förh.* **120**, 315-320.

MEDARIS, L.G., JR., FOURNELLE, J.H. & HENRY, D.J. (2003): Tourmaline-bearing quartz veins in the Baraboo Quartzite, Wisconsin: occurrence and significance of foitite and "oxy-foitite". *Can. Mineral.* **41**, 749-758.

MÖLLER, P. & MUECKE, G.K. (1984): Significance of europium anomalies in silicate melts and crystal–melt equilibria: a re-evaluation. *Contrib. Mineral. Petrol.* **87**, 242-250.

NEIVA, A.M.R. (1974): Geochemistry of tourmaline (schorlite) from granites, aplites and pegmatites from northern Portugal. *Geochim. Cosmochim. Acta* **38**, 1307-1317.

NOVÁK, M., POVONDRA, P. & SELWAY, J.B. (2004): Schorl–oxy-schorl to dravite–oxy-dravite tourmaline from granitic pegmatites; examples from the Moldanubicum, Czech Republic. *Eur. J. Mineral.* **16**, 323-333.

NOVÁK, M., ŠKODA, R., FILIP, J., MACEK, I. & VACULOVIČ, T. (2011): Compositional trends in tourmaline from intragranitic NYF pegmatites of the Třebíč Pluton, Czech Republic: an electron microprobe, Mössbauer and LA–ICP–MS study. *Can. Mineral.* **49**, 359-380.

PESQUERA, A., TORRES-RUIZ, J., GIL-CRESPO, P.P. & JIANG, S.-Y. (2005): Petrographic, chemical and B-isotopic insights into the origin of tourmaline-rich rocks and boron recycling in the Martinamor Antiform (Central Iberian Zone, Salamanca, Spain). *J. Petrol.* **46**, 1013-1044.

PRŠEK, J., ONDREJKA, M., BAČÍK, P., BUDZYŃ, B. & UHER, P. (2010): Metamorphic–hydrothermal REE minerals in the Bacúch magnetite deposit, Western Carpathians, Slovakia: (Sr,S)-rich monazite-(Ce) and Nd-dominant hingganite. *Can. Mineral.* **48**, 81-94.

ROBERTS, S., PALMER, M.R. & WALLER, L. (2006): Sm–Nd and REE characteristics of tourmaline and scheelite from

the Björkdal gold deposit, northern Sweden: evidence of an intrusion-related gold deposit? *Econ. Geol.* **101**, 1415-1425.

RODA, E., PESQUERA, A. & VELASCO, F. (1995): Tourmaline in granitic pegmatites and their country rocks, Fregeneda area, Salamanca, Spain. *Can. Mineral.* **33**, 835-848.

RODA-ROBLES, E., PESQUERA, A., GIL, P.P., TORRES-RUIZ, J. & FONTAN, F. (2004): Tourmaline from the rare-element Pinilla pegmatite, (Central Iberian Zone, Zamora, Spain): chemical variation and implications for pegmatitic evolution. *Mineral. Petrol.* **81**, 249-263.

ROMER, R.L. & SMEDS, S.-A. (1997): U–Pb columbite chronology of post-kinematic Palaeoproterozoic pegmatites in Sweden. *Precamb. Res.* **82**, 85-99.

SHANNON, R.D. (1976): Revised effective ionic radii and systematic studies of interatomic distances in halides and chalcogenides. *Acta Crystallogr.* **A32**, 751-767.

SHELDRICK, G.M. (1997): SHELXL–97, a program for crystal structure refinement. University of Göttingen, Göttingen, Germany.

SMEDS, S.-A. (1990): Regional trends in mineral assemblages of Swedish Proterozoic granitic pegmatites and their geological significance. *Geol. Fören. Stockholm Förh.* **112**, 227-242.

SUNDIUS, N. (1952): Kvarts, fältspat och glimmer samt förekomster därav i Sverige. *Sver. Geol. Undersökning C* **520**.

TORRES-RUIZ, J., PESQUERA, A., GIL-CRESPO, P.P. & VELILLA, N. (2003): Origin and petrogenetic implications of tourmaline-rich rocks in the Sierra Nevada (Betic Cordillera, southeastern Spain). *Chem. Geol.* **197**, 55-86.

YAVUZ, F., ISKENDEROĞLU, A. & JIANG SHAO-YONG (1999): Tourmaline compositions from the Salikvan porphyry Cu–Mo deposit and vicinity, northeastern Turkey. *Can. Mineral.* **37**, 1007-1023.

Received July 22, 2011, revised manuscript accepted July 8, 2012.

```
data_swer_0m

_audit_creation_method            SHELXL-97
_chemical_name_systematic
;
 ?
;
_chemical_name_common             ?
_chemical_melting_point           ?
_chemical_formula_moiety          ?
_chemical_formula_sum
 'H3 Al6.74 B3 Ca0 F0.67 Fe2.26 Mg0 Na0.76 O30.33 Si6'
_chemical_formula_weight          1027.71

loop_
 _atom_type_symbol
 _atom_type_description
 _atom_type_scat_dispersion_real
 _atom_type_scat_dispersion_imag
 _atom_type_scat_source
 'O'  'O'   0.0106   0.0060
 'International Tables Vol C Tables 4.2.6.8 and 6.1.1.4'
 'Na'  'Na'   0.0362   0.0249
 'International Tables Vol C Tables 4.2.6.8 and 6.1.1.4'
 'Mg'  'Mg'   0.0486   0.0363
 'International Tables Vol C Tables 4.2.6.8 and 6.1.1.4'
 'Al'  'Al'   0.0645   0.0514
 'International Tables Vol C Tables 4.2.6.8 and 6.1.1.4'
 'Si'  'Si'   0.0817   0.0704
 'International Tables Vol C Tables 4.2.6.8 and 6.1.1.4'
 'Ca'  'Ca'   0.2262   0.3064
 'International Tables Vol C Tables 4.2.6.8 and 6.1.1.4'
 'Fe'  'Fe'   0.3463   0.8444
 'International Tables Vol C Tables 4.2.6.8 and 6.1.1.4'
 'B'  'B'   0.0013   0.0007
 'International Tables Vol C Tables 4.2.6.8 and 6.1.1.4'
 'H'  'H'   0.0000   0.0000
 'International Tables Vol C Tables 4.2.6.8 and 6.1.1.4'
 'F'  'F'   0.0171   0.0103
 'International Tables Vol C Tables 4.2.6.8 and 6.1.1.4'

_symmetry_cell_setting            ?
_symmetry_space_group_name_H-M    ?

loop_
 _symmetry_equiv_pos_as_xyz
 'x, y, z'
 '-y, x-y, z'
 '-x+y, -x, z'
 '-y, -x, z'
 '-x+y, y, z'
 'x, x-y, z'
 'x+2/3, y+1/3, z+1/3'
 '-y+2/3, x-y+1/3, z+1/3'
```

```
 '-x+y+2/3, -x+1/3, z+1/3'
 '-y+2/3, -x+1/3, z+1/3'
 '-x+y+2/3, y+1/3, z+1/3'
 'x+2/3, x-y+1/3, z+1/3'
 'x+1/3, y+2/3, z+2/3'
 '-y+1/3, x-y+2/3, z+2/3'
 '-x+y+1/3, -x+2/3, z+2/3'
 '-y+1/3, -x+2/3, z+2/3'
 '-x+y+1/3, y+2/3, z+2/3'
 'x+1/3, x-y+2/3, z+2/3'

_cell_length_a                    15.9210(10)
_cell_length_b                    15.9210(10)
_cell_length_c                    7.1750(10)
_cell_angle_alpha                 90.00
_cell_angle_beta                  90.00
_cell_angle_gamma                 120.00
_cell_volume                      1575.0(3)
_cell_formula_units_Z             3
_cell_measurement_temperature     293(2)
_cell_measurement_reflns_used     ?
_cell_measurement_theta_min       ?
_cell_measurement_theta_max       ?

_exptl_crystal_description        ?
_exptl_crystal_colour             ?
_exptl_crystal_size_max           ?
_exptl_crystal_size_mid           ?
_exptl_crystal_size_min           ?
_exptl_crystal_density_meas       ?
_exptl_crystal_density_diffrn     3.250
_exptl_crystal_density_method     'not measured'
_exptl_crystal_F_000              1516
_exptl_absorpt_coefficient_mu     2.368
_exptl_absorpt_correction_type    ?
_exptl_absorpt_correction_T_min   ?
_exptl_absorpt_correction_T_max   ?
_exptl_absorpt_process_details    ?

_exptl_special_details
;
 ?
;

_diffrn_ambient_temperature       293(2)
_diffrn_radiation_wavelength      0.71073
_diffrn_radiation_type            MoK\a
_diffrn_radiation_source          'fine-focus sealed tube'
_diffrn_radiation_monochromator   graphite
_diffrn_measurement_device_type   ?
_diffrn_measurement_method        ?
_diffrn_detector_area_resol_mean  ?
_diffrn_standards_number          ?
_diffrn_standards_interval_count  ?
_diffrn_standards_interval_time   ?
```

```
_diffrn_standards_decay_%         ?
_diffrn_reflns_number             23334
_diffrn_reflns_av_R_equivalents   0.0214
_diffrn_reflns_av_sigmaI/netI     0.0125
_diffrn_reflns_limit_h_min        -28
_diffrn_reflns_limit_h_max        25
_diffrn_reflns_limit_k_min        -28
_diffrn_reflns_limit_k_max        28
_diffrn_reflns_limit_l_min        -13
_diffrn_reflns_limit_l_max        12
_diffrn_reflns_theta_min          2.56
_diffrn_reflns_theta_max          40.27
_reflns_number_total              2370
_reflns_number_gt                 2323
_reflns_threshold_expression      >2sigma(I)

_computing_data_collection        ?
_computing_cell_refinement        ?
_computing_data_reduction         ?
_computing_structure_solution     'SHELXS-97 (Sheldrick, 1990)'
_computing_structure_refinement   'SHELXL-97 (Sheldrick, 1997)'
_computing_molecular_graphics     ?
_computing_publication_material   ?

_refine_special_details
;
 Refinement of F^2^ against ALL reflections.  The weighted R-factor wR and
 goodness of fit S are based on F^2^, conventional R-factors R are based
 on F, with F set to zero for negative F^2^. The threshold expression of
 F^2^ > 2sigma(F^2^) is used only for calculating R-factors(gt) etc. and is
 not relevant to the choice of reflections for refinement.  R-factors based
 on F^2^ are statistically about twice as large as those based on F, and R-
 factors based on ALL data will be even larger.
;

_refine_ls_structure_factor_coef  Fsqd
_refine_ls_matrix_type            full
_refine_ls_weighting_scheme       calc
_refine_ls_weighting_details
 'calc w=1/[\s^2^(Fo^2^)+(0.0200P)^2^+1.9600P] where P=(Fo^2^+2Fc^2^)/3'
_atom_sites_solution_primary      direct
_atom_sites_solution_secondary    difmap
_atom_sites_solution_hydrogens    geom
_refine_ls_hydrogen_treatment     mixed
_refine_ls_extinction_method      SHELXL
_refine_ls_extinction_coef        0.00000(11)
_refine_ls_extinction_expression
 'Fc^*^=kFc[1+0.001xFc^2^\l^3^/sin(2\q)]^-1/4^'
_refine_ls_abs_structure_details
 'Flack H D (1983), Acta Cryst. A39, 876-881'
_refine_ls_abs_structure_Flack    0.06(4)
_refine_ls_number_reflns          2370
_refine_ls_number_parameters      95
_refine_ls_number_restraints      1
_refine_ls_R_factor_all           0.0159
```

```
_refine_ls_R_factor_gt            0.0151
_refine_ls_wR_factor_ref          0.0379
_refine_ls_wR_factor_gt           0.0376
_refine_ls_goodness_of_fit_ref    0.916
_refine_ls_restrained_S_all       0.916
_refine_ls_shift/su_max           1.159
_refine_ls_shift/su_mean          0.012

loop_
 _atom_site_label
 _atom_site_type_symbol
 _atom_site_fract_x
 _atom_site_fract_y
 _atom_site_fract_z
 _atom_site_U_iso_or_equiv
 _atom_site_adp_type
 _atom_site_occupancy
 _atom_site_symmetry_multiplicity
 _atom_site_calc_flag
 _atom_site_refinement_flags
 _atom_site_disorder_assembly
 _atom_site_disorder_group
Na1 Na 1.0000 1.0000 0.23065(19) 0.0193(3) Uani 0.863(6) 6 d SP . .
Fe1 Fe 0.12439(3) 0.062194(13) 0.63110(5) 0.00718(10) Uani 0.0766(13) 2 d SP . .
Mg1 Mg 0.12439(3) 0.062194(13) 0.63110(5) 0.00718(10) Uani 0.92 2 d SP . .
Al2 Al 0.297710(16) 0.261395(17) 0.61062(3) 0.00540(4) Uani 1 1 d . . .
Si1 Si 0.191761(13) 0.189806(14) -0.00040(3) 0.00469(3) Uani 1 1 d . . .
B1 B 0.10976(4) 0.21953(8) 0.45395(15) 0.00598(14) Uani 1 2 d S . .
O1 O 1.0000 1.0000 0.7716(2) 0.0111(2) Uani 1 6 d S . .
O2 O 0.06098(3) 0.12196(6) 0.48629(12) 0.01097(14) Uani 1 2 d S . .
O3 O 0.26378(8) 0.13189(4) 0.50948(12) 0.01269(14) Uani 1 2 d S . .
O4 O 0.09353(3) 0.18707(6) 0.07046(12) 0.00963(12) Uani 1 2 d S . .
O5 O 0.18512(7) 0.09256(3) 0.09237(11) 0.00968(12) Uani 1 2 d S . .
O6 O 0.19549(4) 0.18515(4) 0.77620(7) 0.00792(8) Uani 1 1 d . . .
O7 O 0.28536(4) 0.28518(4) 0.07831(7) 0.00766(8) Uani 1 1 d . . .
O8 O 0.20954(4) 0.27033(4) 0.43993(8) 0.00851(8) Uani 1 1 d . . .
H1 H 0.2592(19) 0.1296(10) 0.402(4) 0.034(7) Uiso 1 2 d S . .

loop_
 _atom_site_aniso_label
 _atom_site_aniso_U_11
 _atom_site_aniso_U_22
 _atom_site_aniso_U_33
 _atom_site_aniso_U_23
 _atom_site_aniso_U_13
 _atom_site_aniso_U_12
Na1 0.0191(4) 0.0191(4) 0.0197(6) 0.000 0.000 0.0096(2)
Fe1 0.00682(15) 0.00470(11) 0.01074(16) -0.00172(5) -0.00344(10) 0.00341(7)
Mg1 0.00682(15) 0.00470(11) 0.01074(16) -0.00172(5) -0.00344(10) 0.00341(7)
Al2 0.00528(8) 0.00555(8) 0.00533(7) 0.00038(6) -0.00007(6) 0.00267(7)
Si1 0.00462(7) 0.00423(7) 0.00521(7) -0.00060(6) -0.00044(6) 0.00220(5)
B1 0.0052(3) 0.0057(4) 0.0071(4) 0.0007(3) 0.00034(14) 0.00286(18)
O1 0.0131(3) 0.0131(3) 0.0071(5) 0.000 0.000 0.00655(17)
O2 0.0126(3) 0.0050(3) 0.0127(3) 0.0002(2) 0.00010(11) 0.00252(13)
O3 0.0246(4) 0.0120(2) 0.0057(3) 0.00008(14) 0.0002(3) 0.0123(2)
```

```
O4 0.00715(19) 0.0145(3) 0.0097(3) -0.0015(3) -0.00075(13) 0.00727(17)
O5 0.0150(3) 0.00726(19) 0.0093(3) 0.00088(12) 0.0018(2) 0.00750(17)
O6 0.0093(2) 0.0098(2) 0.00527(18) -0.00128(15) -0.00083(15) 0.00521(17)
O7 0.00649(19) 0.00625(18) 0.00760(19) -0.00101(15) -0.00103(15) 0.00121(15)
O8 0.00467(18) 0.0090(2) 0.0118(2) 0.00257(16) 0.00093(16) 0.00336(16)

_geom_special_details
;
 All esds (except the esd in the dihedral angle between two l.s. planes)
 are estimated using the full covariance matrix.  The cell esds are taken
 into account individually in the estimation of esds in distances, angles
 and torsion angles; correlations between esds in cell parameters are only
 used when they are defined by crystal symmetry.  An approximate (isotropic)
 treatment of cell esds is used for estimating esds involving l.s. planes.
;

loop_
 _geom_bond_atom_site_label_1
 _geom_bond_atom_site_label_2
 _geom_bond_distance
 _geom_bond_site_symmetry_2
 _geom_bond_publ_flag
Na1 O2 2.4884(13) 1_665 ?
Na1 O2 2.4884(13) 2_665 ?
Na1 O2 2.4884(13) 3_665 ?
Na1 O5 2.7385(10) 2_665 ?
Na1 O5 2.7385(10) 3_665 ?
Na1 O5 2.7385(10) 1_665 ?
Na1 O4 2.8237(11) 2_665 ?
Na1 O4 2.8237(11) 1_665 ?
Na1 O4 2.8237(11) 3_665 ?
Na1 Mg1 3.3462(13) 1_665 ?
Na1 Fe1 3.3462(13) 1_665 ?
Na1 Mg1 3.3462(13) 2_665 ?
Fe1 O2 1.9911(6) 3 ?
Fe1 O2 1.9911(6) . ?
Fe1 O6 1.9953(6) . ?
Fe1 O6 1.9953(6) 6 ?
Fe1 O1 1.9894(8) 1_445 ?
Fe1 O3 2.1108(11) . ?
Fe1 Al2 2.9905(4) . ?
Fe1 Al2 2.9905(4) 6 ?
Fe1 Mg1 2.9706(7) 3 ?
Fe1 Mg1 2.9706(7) 2 ?
Fe1 Na1 3.3462(13) 1_445 ?
Al2 O6 1.8863(6) . ?
Al2 O7 1.8984(6) 8 ?
Al2 O8 1.8922(6) 8 ?
Al2 O8 1.9210(6) . ?
Al2 O7 1.9532(6) 15 ?
Al2 O3 1.9889(5) . ?
Al2 Al2 2.9447(4) 15_554 ?
Al2 Al2 2.9448(4) 8 ?
Si1 O7 1.6070(5) . ?
Si1 O6 1.6071(6) 1_554 ?
```

```
Si1 O4 1.6242(3) . ?
Si1 O5 1.6394(4) . ?
Si1 Mg1 3.1764(5) 1_554 ?
Si1 Na1 3.4605(7) 1_445 ?
B1 O2 1.3651(14) . ?
B1 O8 1.3794(8) 5 ?
B1 O8 1.3794(8) . ?
B1 Mg1 2.9202(9) 2 ?
O1 Mg1 1.9894(8) 2_665 ?
O1 Fe1 1.9894(8) 2_665 ?
O1 Mg1 1.9894(8) 3_665 ?
O1 Fe1 1.9894(8) 3_665 ?
O1 Mg1 1.9894(8) 1_665 ?
O1 Fe1 1.9894(8) 1_665 ?
O2 Mg1 1.9911(6) 2 ?
O2 Fe1 1.9911(6) 2 ?
O2 Na1 2.4884(13) 1_445 ?
O3 Al2 1.9889(5) 6 ?
O3 H1 0.78(3) . ?
O4 Si1 1.6242(3) 5 ?
O4 Na1 2.8237(11) 1_445 ?
O5 Si1 1.6394(4) 6 ?
O5 Na1 2.7385(10) 1_445 ?
O6 Si1 1.6071(6) 1_556 ?
O7 Al2 1.8984(6) 15_554 ?
O7 Al2 1.9532(6) 8_554 ?
O8 Al2 1.8922(6) 15_554 ?

loop_
 _geom_angle_atom_site_label_1
 _geom_angle_atom_site_label_2
 _geom_angle_atom_site_label_3
 _geom_angle
 _geom_angle_site_symmetry_1
 _geom_angle_site_symmetry_3
 _geom_angle_publ_flag
O2 Na1 O2 71.64(5) 1_665 2_665 ?
O2 Na1 O2 71.64(5) 1_665 3_665 ?
O2 Na1 O2 71.64(5) 2_665 3_665 ?
O2 Na1 O5 87.26(2) 1_665 2_665 ?
O2 Na1 O5 87.26(2) 2_665 2_665 ?
O2 Na1 O5 153.75(5) 3_665 2_665 ?
O2 Na1 O5 153.75(5) 1_665 3_665 ?
O2 Na1 O5 87.26(2) 2_665 3_665 ?
O2 Na1 O5 87.26(2) 3_665 3_665 ?
O5 Na1 O5 107.65(3) 2_665 3_665 ?
O2 Na1 O5 87.26(2) 1_665 1_665 ?
O2 Na1 O5 153.75(5) 2_665 1_665 ?
O2 Na1 O5 87.26(2) 3_665 1_665 ?
O5 Na1 O5 107.65(3) 2_665 1_665 ?
O5 Na1 O5 107.65(3) 3_665 1_665 ?
O2 Na1 O4 127.49(2) 1_665 2_665 ?
O2 Na1 O4 71.50(3) 2_665 2_665 ?
O2 Na1 O4 127.49(2) 3_665 2_665 ?
O5 Na1 O4 55.030(12) 2_665 2_665 ?
```

```
O5 Na1 O4 55.030(12) 3_665 2_665 ?
O5 Na1 O4 134.74(6) 1_665 2_665 ?
O2 Na1 O4 71.50(3) 1_665 1_665 ?
O2 Na1 O4 127.49(2) 2_665 1_665 ?
O2 Na1 O4 127.49(2) 3_665 1_665 ?
O5 Na1 O4 55.030(12) 2_665 1_665 ?
O5 Na1 O4 134.74(6) 3_665 1_665 ?
O5 Na1 O4 55.030(12) 1_665 1_665 ?
O4 Na1 O4 104.57(3) 2_665 1_665 ?
O2 Na1 O4 127.49(2) 1_665 3_665 ?
O2 Na1 O4 127.49(2) 2_665 3_665 ?
O2 Na1 O4 71.50(3) 3_665 3_665 ?
O5 Na1 O4 134.74(6) 2_665 3_665 ?
O5 Na1 O4 55.030(12) 3_665 3_665 ?
O5 Na1 O4 55.030(12) 1_665 3_665 ?
O4 Na1 O4 104.57(3) 2_665 3_665 ?
O4 Na1 O4 104.57(3) 1_665 3_665 ?
O2 Na1 Mg1 36.28(2) 1_665 1_665 ?
O2 Na1 Mg1 73.35(4) 2_665 1_665 ?
O2 Na1 Mg1 36.28(2) 3_665 1_665 ?
O5 Na1 Mg1 123.36(3) 2_665 1_665 ?
O5 Na1 Mg1 123.36(3) 3_665 1_665 ?
O5 Na1 Mg1 80.41(2) 1_665 1_665 ?
O4 Na1 Mg1 144.85(4) 2_665 1_665 ?
O4 Na1 Mg1 96.63(2) 1_665 1_665 ?
O4 Na1 Mg1 96.63(2) 3_665 1_665 ?
O2 Na1 Fe1 36.28(2) 1_665 1_665 ?
O2 Na1 Fe1 73.35(4) 2_665 1_665 ?
O2 Na1 Fe1 36.28(2) 3_665 1_665 ?
O5 Na1 Fe1 123.36(3) 2_665 1_665 ?
O5 Na1 Fe1 123.36(3) 3_665 1_665 ?
O5 Na1 Fe1 80.41(2) 1_665 1_665 ?
O4 Na1 Fe1 144.85(4) 2_665 1_665 ?
O4 Na1 Fe1 96.63(2) 1_665 1_665 ?
O4 Na1 Fe1 96.63(2) 3_665 1_665 ?
Mg1 Na1 Fe1 0.000(10) 1_665 1_665 ?
O2 Na1 Mg1 36.28(2) 1_665 2_665 ?
O2 Na1 Mg1 36.28(2) 2_665 2_665 ?
O2 Na1 Mg1 73.35(4) 3_665 2_665 ?
O5 Na1 Mg1 80.41(2) 2_665 2_665 ?
O5 Na1 Mg1 123.36(3) 3_665 2_665 ?
O5 Na1 Mg1 123.36(3) 1_665 2_665 ?
O4 Na1 Mg1 96.63(2) 2_665 2_665 ?
O4 Na1 Mg1 96.63(2) 1_665 2_665 ?
O4 Na1 Mg1 144.85(4) 3_665 2_665 ?
Mg1 Na1 Mg1 52.70(2) 1_665 2_665 ?
Fe1 Na1 Mg1 52.70(2) 1_665 2_665 ?
O2 Fe1 O2 94.01(5) 3 . ?
O2 Fe1 O6 176.43(3) 3 . ?
O2 Fe1 O6 88.73(3) . . ?
O2 Fe1 O6 88.73(3) 3 6 ?
O2 Fe1 O6 176.43(3) . 6 ?
O6 Fe1 O6 88.44(4) . 6 ?
O2 Fe1 O1 83.45(3) 3 1_445 ?
O2 Fe1 O1 83.45(3) . 1_445 ?
```

```
O6 Fe1 O1 99.16(3) . 1_445 ?
O6 Fe1 O1 99.16(3) 6 1_445 ?
O2 Fe1 O3 100.61(3) 3 . ?
O2 Fe1 O3 100.61(3) . . ?
O6 Fe1 O3 76.61(3) . . ?
O6 Fe1 O3 76.61(3) 6 . ?
O1 Fe1 O3 173.97(5) 1_445 . ?
O2 Fe1 Al2 139.77(3) 3 . ?
O2 Fe1 Al2 83.51(2) . . ?
O6 Fe1 Al2 38.295(18) . . ?
O6 Fe1 Al2 92.92(2) 6 . ?
O1 Fe1 Al2 135.55(2) 1_445 . ?
O3 Fe1 Al2 41.586(12) . . ?
O2 Fe1 Al2 83.51(2) 3 6 ?
O2 Fe1 Al2 139.77(3) . 6 ?
O6 Fe1 Al2 92.92(2) . 6 ?
O6 Fe1 Al2 38.295(18) 6 6 ?
O1 Fe1 Al2 135.55(2) 1_445 6 ?
O3 Fe1 Al2 41.586(12) . 6 ?
Al2 Fe1 Al2 73.618(12) . 6 ?
O2 Fe1 Mg1 41.76(2) 3 3 ?
O2 Fe1 Mg1 89.17(2) . 3 ?
O6 Fe1 Mg1 140.73(2) . 3 ?
O6 Fe1 Mg1 94.403(18) 6 3 ?
O1 Fe1 Mg1 41.70(2) 1_445 3 ?
O3 Fe1 Mg1 142.051(15) . 3 ?
Al2 Fe1 Mg1 172.586(6) . 3 ?
Al2 Fe1 Mg1 113.109(6) 6 3 ?
O2 Fe1 Mg1 89.17(2) 3 2 ?
O2 Fe1 Mg1 41.76(2) . 2 ?
O6 Fe1 Mg1 94.404(18) . 2 ?
O6 Fe1 Mg1 140.73(2) 6 2 ?
O1 Fe1 Mg1 41.70(2) 1_445 2 ?
O3 Fe1 Mg1 142.051(15) . 2 ?
Al2 Fe1 Mg1 113.109(6) . 2 ?
Al2 Fe1 Mg1 172.586(6) 6 2 ?
Mg1 Fe1 Mg1 60.0 3 2 ?
O2 Fe1 Na1 47.69(3) 3 1_445 ?
O2 Fe1 Na1 47.69(3) . 1_445 ?
O6 Fe1 Na1 134.414(18) . 1_445 ?
O6 Fe1 Na1 134.414(18) 6 1_445 ?
O1 Fe1 Na1 89.61(4) 1_445 1_445 ?
O3 Fe1 Na1 96.41(3) . 1_445 ?
Al2 Fe1 Na1 111.555(15) . 1_445 ?
Al2 Fe1 Na1 111.555(15) 6 1_445 ?
Mg1 Fe1 Na1 63.649(12) 3 1_445 ?
Mg1 Fe1 Na1 63.649(12) 2 1_445 ?
O6 Al2 O7 169.13(3) . 8 ?
O6 Al2 O8 94.61(3) . 8 ?
O7 Al2 O8 96.20(3) 8 8 ?
O6 Al2 O8 91.25(3) . . ?
O7 Al2 O8 78.13(2) 8 . ?
O8 Al2 O8 171.53(2) 8 . ?
O6 Al2 O7 93.03(3) . 15 ?
O7 Al2 O7 90.442(13) 8 15 ?
```

```
O8 Al2 O7 77.48(2) 8 15 ?
O8 Al2 O7 96.14(3) . 15 ?
O6 Al2 O3 82.12(3) . . ?
O7 Al2 O3 95.58(3) 8 . ?
O8 Al2 O3 96.01(3) 8 . ?
O8 Al2 O3 90.83(3) . . ?
O7 Al2 O3 171.61(3) 15 . ?
O6 Al2 Al2 129.26(2) . 15_554 ?
O7 Al2 Al2 40.824(17) 8 15_554 ?
O8 Al2 Al2 133.67(2) 8 15_554 ?
O8 Al2 Al2 39.090(18) . 15_554 ?
O7 Al2 Al2 85.17(2) 15 15_554 ?
O3 Al2 Al2 103.21(2) . 15_554 ?
O6 Al2 Al2 85.829(19) . 8 ?
O7 Al2 Al2 103.28(2) 8 8 ?
O8 Al2 Al2 39.800(19) 8 8 ?
O8 Al2 Al2 135.00(2) . 8 ?
O7 Al2 Al2 39.450(16) 15 8 ?
O3 Al2 Al2 132.85(3) . 8 ?
Al2 Al2 Al2 119.304(12) 15_554 8 ?
O6 Al2 Fe1 40.959(19) . . ?
O7 Al2 Fe1 132.46(2) 8 . ?
O8 Al2 Fe1 110.59(2) 8 . ?
O8 Al2 Fe1 77.811(19) . . ?
O7 Al2 Fe1 132.43(2) 15 . ?
O3 Al2 Fe1 44.78(3) . . ?
Al2 Al2 Fe1 112.760(12) 15_554 . ?
Al2 Al2 Fe1 122.616(11) 8 . ?
O7 Si1 O6 110.85(3) . 1_554 ?
O7 Si1 O4 109.93(4) . . ?
O6 Si1 O4 111.61(4) 1_554 . ?
O7 Si1 O5 109.94(4) . . ?
O6 Si1 O5 110.35(4) 1_554 . ?
O4 Si1 O5 103.94(4) . . ?
O7 Si1 Mg1 138.93(2) . 1_554 ?
O6 Si1 Mg1 31.65(2) 1_554 1_554 ?
O4 Si1 Mg1 103.34(3) . 1_554 ?
O5 Si1 Mg1 83.81(3) . 1_554 ?
O7 Si1 Na1 130.78(3) . 1_445 ?
O6 Si1 Na1 118.31(3) 1_554 1_445 ?
O4 Si1 Na1 53.80(3) . 1_445 ?
O5 Si1 Na1 50.85(3) . 1_445 ?
Mg1 Si1 Na1 88.39(2) 1_554 1_445 ?
O2 B1 O8 120.85(4) . 5 ?
O2 B1 O8 120.85(4) . . ?
O8 B1 O8 118.28(9) 5 . ?
O2 B1 Mg1 36.29(3) . 2 ?
O8 B1 Mg1 88.41(4) 5 2 ?
O8 B1 Mg1 147.73(6) . 2 ?
Mg1 O1 Fe1 0.000(8) 2_665 2_665 ?
Mg1 O1 Mg1 96.59(5) 2_665 3_665 ?
Fe1 O1 Mg1 96.59(5) 2_665 3_665 ?
Mg1 O1 Fe1 96.59(5) 2_665 3_665 ?
Fe1 O1 Fe1 96.59(5) 2_665 3_665 ?
Mg1 O1 Fe1 0.000(12) 3_665 3_665 ?
```

```
Mg1 O1 Mg1 96.59(5) 2_665 1_665 ?
Fe1 O1 Mg1 96.59(5) 2_665 1_665 ?
Mg1 O1 Mg1 96.59(5) 3_665 1_665 ?
Fe1 O1 Mg1 96.59(5) 3_665 1_665 ?
Mg1 O1 Fe1 96.59(5) 2_665 1_665 ?
Fe1 O1 Fe1 96.59(5) 2_665 1_665 ?
Mg1 O1 Fe1 96.59(5) 3_665 1_665 ?
Fe1 O1 Fe1 96.59(5) 3_665 1_665 ?
Mg1 O1 Fe1 0.000(18) 1_665 1_665 ?
B1 O2 Mg1 119.77(4) . 2 ?
B1 O2 Fe1 119.77(4) . 2 ?
Mg1 O2 Fe1 0.000(8) 2 2 ?
B1 O2 Fe1 119.77(4) . . ?
Mg1 O2 Fe1 96.48(4) 2 . ?
Fe1 O2 Fe1 96.48(4) 2 . ?
B1 O2 Na1 122.73(7) . 1_445 ?
Mg1 O2 Na1 96.02(3) 2 1_445 ?
Fe1 O2 Na1 96.02(3) 2 1_445 ?
Fe1 O2 Na1 96.02(3) . 1_445 ?
Al2 O3 Al2 128.55(5) . 6 ?
Al2 O3 Fe1 93.63(3) . . ?
Al2 O3 Fe1 93.63(3) 6 . ?
Al2 O3 H1 112.5(4) . . ?
Al2 O3 H1 112.5(4) 6 . ?
Fe1 O3 H1 110(2) . . ?
Si1 O4 Si1 143.41(6) 5 . ?
Si1 O4 Na1 98.55(3) 5 1_445 ?
Si1 O4 Na1 98.55(3) . 1_445 ?
Si1 O5 Si1 131.61(5) 6 . ?
Si1 O5 Na1 101.49(3) 6 1_445 ?
Si1 O5 Na1 101.49(3) . 1_445 ?
Si1 O6 Al2 129.67(3) 1_556 . ?
Si1 O6 Fe1 123.35(3) 1_556 . ?
Al2 O6 Fe1 100.75(3) . . ?
Si1 O7 Al2 130.30(3) . 15_554 ?
Si1 O7 Al2 127.05(3) . 8_554 ?
Al2 O7 Al2 99.72(2) 15_554 8_554 ?
B1 O8 Al2 133.28(6) . 15_554 ?
B1 O8 Al2 125.46(6) . . ?
Al2 O8 Al2 101.11(3) 15_554 . ?

_diffrn_measured_fraction_theta_max    0.998
_diffrn_reflns_theta_full              40.27
_diffrn_measured_fraction_theta_full   0.998
_refine_diff_density_max    0.359
_refine_diff_density_min   -0.267
_refine_diff_density_rms    0.068
```